

## THE NEUTRINO BUBBLE INSTABILITY: A MECHANISM FOR GENERATING PULSAR KICKS

ARISTOTLE SOCRATES,<sup>1,2</sup> OMER BLAES,<sup>3</sup> AIMEE HUNGERFORD<sup>4</sup>, AND CHRIS L. FRYER<sup>5</sup>  
*Draft version September 1, 2018*

### ABSTRACT

An explanation for the large random velocities of pulsars is presented. Like many other models, we propose that the momentum imparted to the star is given at birth. The ultimate source of energy is provided by the intense optically thick neutrino flux that is responsible for radiating the proto-neutron star’s gravitational binding energy during the Kelvin-Helmholtz phase. The central feature of the kick mechanism is a radiative-driven magnetoacoustic instability, which we refer to as “neutrino bubbles.” Identical in nature to the photon bubble instability, the neutrino bubble instability requires the presence of an equilibrium radiative flux as well as a coherent steady background magnetic field. Over regions of large magnetic flux densities, the neutrino bubble instability is allowed to grow on dynamical timescales  $\sim 1$ ms, potentially leading to large luminosity enhancements and density fluctuations. Local luminosity enhancements, which preferentially occur over regions of strong magnetic field, lead to a net global asymmetry in the neutrino emission and the young neutron star is propelled in the direction opposite to these regions. For favorable values of magnetic field structure, size, and strength as well as neutrino bubble saturation amplitude, momentum kicks in excess of  $1000 \text{ km s}^{-1}$  can be achieved. Since the neutrino-powered kick is delivered over the duration of the Kelvin-Helmholtz time  $\sim$  a few seconds, one expects spin-kick alignment from this neutrino bubble powered model.

*Subject headings:* stars:evolution–stars:oscillations–MHD–instabilities–gravitational waves–pulsars:general

### 1. INTRODUCTION

Shortly after their discovery, it was understood that neutron stars travel with random velocities significantly in excess of the massive stars from which they were born (Gunn & Ostriker 1971). More recently, studies of pulsar velocity distributions suggest that neutron stars indeed possess large proper motions and that the momentum kick is most likely given at birth possibly with a bimodal velocity distribution (Lyne & Lorimer 1994; Lorimer, Bailes, & Harrison 1997; Fryer, Burrows, & Benz 1998; Cordes & Chernoff 1998; Arzoumanian, Chernoff, & Cordes 2002). The orbital behavior of individual double neutron star and black hole systems also imply that neutron stars receive natal kicks (Fryer & Kalogera 1997; Kramer 1998; Tauris et al. 1999; Wex, Kalogera, & Kramer 2000; Mirabel et al. 2002).

From a theoretical point of view, a natal kick is a reasonable outcome of stellar collapse and the subsequent explosion. Approximately  $10^{51}$  erg of kinetic energy is released by the prompt explosion mechanism, which can be thought of as a shell of  $\sim 10^{-1} M_{\odot}$  traveling radially outward at  $\sim 10^9 \text{ cm s}^{-1}$ . Thus, a momentum asymmetry in the shock of  $\sim 10\%$  could potentially endow a neutron star with a kick velocity  $\sim 10^8 \text{ cm s}^{-1} = 10^3 \text{ km s}^{-1}$ . Motivated by this simple kinematic argument, Burrows & Hayes (1996) pursued a “hydrodynamically-driven” kick mechanism by artificially deforming the outer portions of an Fe core progenitor and numerically evolving the subsequent collapse and bounce. They found that a “mass-rocket” produced a kick of  $\sim 500 \text{ km s}^{-1}$ . One possibility for a substantial seed asymmetry may be due to unstable  $g$ -modes in progenitor Fe core, which are driven by the  $\epsilon$ -mechanism in the outer shell (Lai & Goldreich 2000).

The intense optically thick neutrino radiation is another potential reservoir of energy for natal kicks. During the Kelvin-Helmholtz phase, neutrino emission is responsible for radiating  $\sim 99\%$  of the star’s gravitational binding energy, which amounts to  $\sim$  a few  $\times 10^{53}$  erg. Asymmetric neutrino surface emission of order  $\sim$  a few% leads to a kick of  $\sim 10^3 \text{ km s}^{-1}$ . The magnetic field of a proto-neutron star may provide the needed systematic asymmetry in such a profoundly spherically symmetric environment, in which the neutrinos can couple. Since the weak interaction violates parity conservation, the neutrinos preferentially scatter towards one magnetic pole over the other. This “neutrino/magnetic-driven” mechanism requires global magnetic field strengths  $\sim 10^{16} \text{ G}$  in order to produce a kick of  $\sim 10^3 \text{ km s}^{-1}$  (Arras & Lai 1999a, 1999b).

In this paper, we describe an alternative model for neutron star kicks that can be viewed, in the broadest sense, as a synthesis of the hydrodynamic- and neutrino/magnetic- driven models. By considering general radiative envelopes that are stratified, optically thick, magnetized, and highly electrically conducting, Blaes & Socrates (2003, hereafter BS03) showed that local magnetoacoustic perturbations are susceptible to radiative driving, a phenomenon known as “photon bubbles” (Arons 1992; Gammie 1998). The non-linear evolution of the photon bubble instability is far from certain as research of this phenomenon is in the developmental stages (Begelman 2001, Turner et al. 2004). Regardless, it is reasonable to suspect that radiative flux enhancements occur in the saturated state since

<sup>1</sup> Department of Astrophysical Sciences, Princeton University, Peyton Hall-Ivy Lane, Princeton, NJ 08544: socrates@astro.princeton.edu and Department of Physics, University of California, Santa Barbara, CA 93106

<sup>2</sup> Hubble Fellow

<sup>3</sup> Department of Physics, University of California, Santa Barbara, CA 93106: blaes@physics.ucsb.edu

<sup>4</sup> Transport Methods, Los Alamos National Laboratory, Los Alamos, NM 87545: aimee@lanl.gov and The University of Arizona, Tucson, AZ 85721

<sup>5</sup> Theoretical Astrophysics, Los Alamos National Laboratory, Los Alamos, NM 87545: fryer@lanl.gov and Physics Department, The University of Arizona, Tucson, AZ 85721

the radiative flux provides the free energy for the instability. In the case of proto-neutron star atmospheres, *neutrino bubbles* rather than photon bubbles may vigorously operate in surface regions that are substantially magnetized since neutrinos rather than photons are the particle species responsible for the diffusive transfer of energy. Over these regions, neutrino flux enhancements propel the star in the opposite direction, potentially providing a natal kick (See Figure 1). In a way, one can view this mechanism as a “neutrino magnetohydrodynamically-driven” mechanism. The main focus of this work is to understand the mechanics, thermodynamics, and stability properties of local radiation magnetohydrodynamic oscillations in proto-neutron stars so that we can assess the feasibility, to first approximation, of a neutrino bubble powered kick mechanism.

The organization of this paper is as follows. In §2 we provide some initial theoretical arguments in order to motivate this work. The importance of radiation-driven fluid instabilities is stressed by comparing the envelope structure of proto-neutron stars with those on the main sequence. Based on the magnetic field structure of the solar convection zone, we describe magnetic field configurations on the surface of proto-neutron stars that are favorable for neutrino bubble powered kicks. A detailed analysis of local magnetoacoustic perturbations in the limit of rapid neutrino diffusion is carried out in §§3-5. Our simplifying assumptions and problem set up are sketched out in §3. The thermodynamic behavior of short-wavelength oscillations in degenerate radiating fluids is investigated in §4. The driving mechanism of the neutrino bubble instability is presented §5 in terms of the relationship between pressure and density as well as force and velocity. Also in §5, the neutrino bubble stability criterion is evaluated in terms of parameters relevant for proto-neutron star surfaces. A Monte Carlo radiation transfer study is performed in §6 where we estimate the value of the kick as well as the gravitational wave strain produced by the globally asymmetric neutrino radiation. A comparison to other kick mechanisms and a critical summary are given in §7.

## 2. THE KICK MECHANISM

A proto-neutron star (PNS) releases  $\sim 99\%$  of the accumulated binding energy from its Fe core progenitor in the form of neutrinos. The neutrinos escape the PNS nearly uniformly across all neutrino flavors during the Kelvin-Helmholtz phase, which lasts for  $\sim 10$ s after its birth. If the neutrino emission is asymmetric by roughly a few percent, the PNS receives a natal kick  $\sim 10^3 \text{ km s}^{-1}$  (Arras & Lai 1999a). Since the neutrino emission by far dominates the energetics during the Kelvin-Helmholtz phase, the main difficulty in formulating a neutrino-powered kick model rests in identifying an intrinsic systematic asymmetry in which the neutrinos can couple.

A natural candidate for inducing a neutrino asymmetry is the magnetic field of the PNS. On their own, magnetic fields alter neutrino-nucleon scattering and absorption via coupling between the background field and the nucleon’s magnetic dipole moment. Since the weak interaction violates parity, the introduction of an axial magnetic field into the scattering matrix causes the neutrinos to preferentially scatter toward one magnetic pole over the other. However, this effect exists only as long as neutrinos are allowed to deviate from local thermal and chemical equilibrium (Arras & Lai 1999a). At and above this layer, neutrinos begin to mechanically decouple from the matter as well, implying a lack of momentum exchange between the neutrinos and the entire PNS. Thus, strong  $\sim 10^{16} \text{ G}$  global magnetic fields are required to induce a significant neutrino asymmetry above the energy decoupling layer.

Here, we also exploit the magnetic field for the purpose of generating neutrino-powered natal kicks. Rather than altering the thermal transport properties of neutrinos, we propose that the magnetic field induces a radiation-driven fluid instability at and below the neutrinosphere. The fluid instability is acoustic in nature and is driven in the exact same way as the “photon bubble” instabilities, which may operate in neutron star accretion caps, relativistic accretion disks, and magnetized main sequence stellar envelopes (Arons 1992, Gammie 1998, BS03). In the case of PNSs, neutrinos are the species with relatively large mean free paths and therefore enable the diffusive transport of energy. It follows that in the envelopes of PNSs, the *neutrino* bubble instability is the relevant mechanism when considering radiative magnetosonic stability. As the instability grows and saturates, a luminosity perturbation is induced about regions of large magnetic flux density and the PNS is propelled in the direction opposite to these “starspots.”

In order for a radiation-driven fluid instability to saturate with a large luminosity perturbation, one expects the radiation pressure to be at least comparable in value to the gas pressure. For PNSs, the average neutrino luminosity during the Kelvin-Helmholtz era is  $\sim 0.01$  the Eddington value, implying that the equilibrium radiation pressure is  $\sim 0.01$  the equilibrium gas pressure. However, at and below the neutrinosphere, the radiation and neutrinos are in thermal and chemical equilibrium with one another on the dynamical timescales of interest, which are of order 1 ms – the acoustic crossing time over a gas pressure scale height. We will demonstrate that the spatial distribution of both temperature and neutrino chemical potential for a given acoustic MHD mode are responsible for driving the neutrino bubble instability. Since the temperature and relative composition of the gas are locked to that of the neutrinos, the gas itself behaves in a fashion similar to the radiation and provides for the majority of the driving. It follows that at least to linear order, the stress responsible for radiative driving is comparable in magnitude to the acoustic restoring force, opening up the possibility for large saturation amplitudes.

Radiation-driven acoustic instabilities, e.g. the  $\kappa$ -mechanism, are ultimately driven by the background radiation flux coupling to the fluid displacement and density perturbation. Yet, damping from radiative diffusion only depends on the total pressure of the gas. The larger the ratio of flux to pressure, the more likely driving will overcome damping. In other words, as the radiation field becomes increasingly anisotropic, the free energy per quanta available for acoustic driving increases accordingly. Due to their stiff equation of state above nuclear saturation density and the relatively low number of total optical depths  $\sim$  a few thousand, the radiation fields of PNSs are highly anisotropic in comparison to those of main sequence stars whose luminosities are  $\sim 0.01 L_{\text{edd}}$  in photons. To illustrate this point, compare the fraction of stellar mass lying one optical depth below the surface of last scattering for a PNS and a  $4M_{\odot}$  A-star

$$\begin{aligned} \text{PROTO-NEUTRON STAR}(0.01 L_{\text{edd}}) : \quad \frac{\delta M}{M_{\odot}} &\sim \frac{R_{\nu}^2 H_{\nu} \rho_{\nu}}{R_{\nu}^3 \rho_c} = 10^{-4} \left( \frac{H_{\nu}}{1 \text{ km}} \right) \left( \frac{10 \text{ km}}{R_{\nu}} \right) \left( \frac{\rho_{\nu}}{10^{11} \text{ g cm}^{-3}} \right) \left( \frac{10^{14} \text{ g cm}^{-3}}{\rho_c} \right) \\ \text{MAIN SEQUENCE STAR}(0.01 L_{\text{edd}}) : \quad \frac{\delta M}{M_{\odot}} &\sim \frac{R_*^2 H_* \rho_*}{R_*^3 \rho_c} = 10^{-11} \left( \frac{H_*}{10^2 \text{ km}} \right) \left( \frac{10^5 \text{ km}}{R_*} \right) \left( \frac{\rho_*}{10^{-7} \text{ g cm}^{-3}} \right) \left( \frac{10 \text{ g cm}^{-3}}{\rho_c} \right) \quad (1) \end{aligned}$$

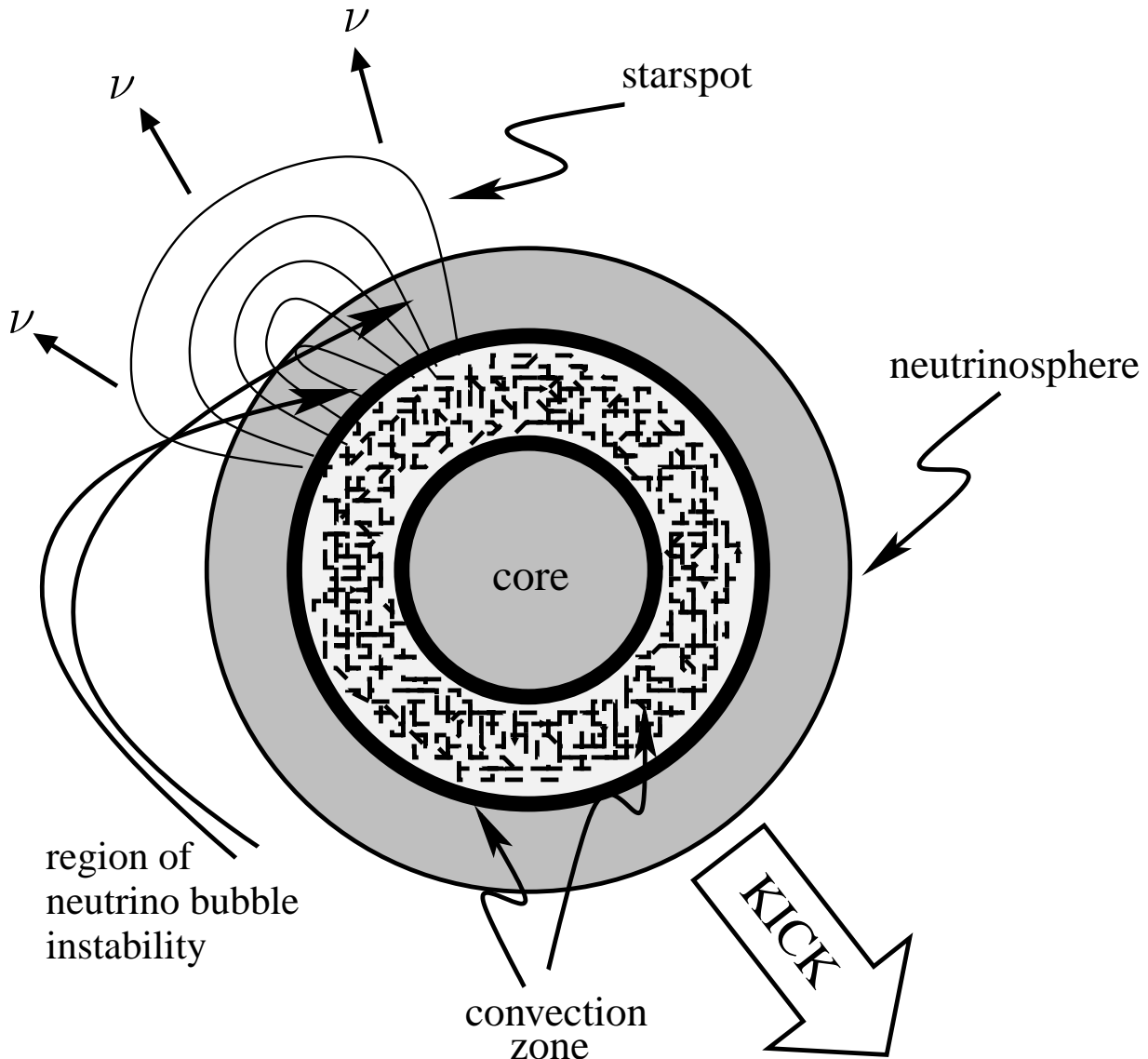


FIG. 1.— Sketch of the kick mechanism. Starspot-like magnetic field structures are generated at the base of convection zone and are transported to the upper-base of the convection zone by both buoyancy and turbulent pumping in a few overturn times. If the presence of strong, long-lived, large scale magnetic “starspots” can induce neutrino bubble instability for a significant fraction of the Kelvin-Helmholtz time, the proto-neutron star will receive a natal kick due to enhanced neutrino transport in the vicinity of the starspot. For average initial rotation rates and random starspot placement, the rotation axis will most likely be aligned with the kick for a given neutron star.

where  $R_i$ ,  $H_i$ ,  $\rho_i$ , and  $\rho_c$  is the radius of the surface of last scattering, the scale height of the surface of last scattering, the density at the last scattering surface, and the central core density, respectively. From the above argument, one suspects that a greater fraction of the total stellar mass is responsible for radiative-acoustic driving in PNSs than in main sequence stars of comparable Eddington factors. Thus, PNSs are promising sights for radiation-driven acoustic instability of any type since a larger mass fraction responsible for driving implies a relatively large luminosity perturbation. If, for example, the  $\kappa$ -mechanism (Baker & Kippenhahn 1962, Unno et al. 1989) or strange modes (Glatzel 1994) operate in the envelopes of PNSs, large luminosity perturbations may follow. An increase in the overall integrated luminosity of  $\sim 10\%$  during the first few hundred milliseconds may significantly contribute to the explosion mechanism. Since the focus of this work is centered on producing a potential kick mechanism, our analysis will be heavily weighted toward radiation-MHD driving mechanisms which are only located on patches of large magnetic flux density.

The nature of the magnetic field structures in the vicinity of the neutrinosphere in part, determines whether or not neutrino bubble instability can power kicks, or even explosions. In the following discussion, mainly phenomenological arguments are put forth in order to motivate the *possibility* that coherent magnetic formations can exist for a substantial fraction of the Kelvin-Helmholtz time while covering a sizable fraction of the star, with large ( $10^{14} - 10^{15}$ G) field strengths.

### 2.1. Convection and Magnetism in Proto-Neutron Stars

It is believed that PNSs convect as they cool. At very early times the escaping shock dissociates ambient nuclei into baryons, heating the mantle while producing a negative entropy gradient that drives convection (Bethe, Brown & Cooperstein 1987; Wilson & Mayle 1988). Due to their large energies and mean free paths, neutrinos radiate the entropy excess left over by the prompt shock, immediately quenching the convection in  $\lesssim 100$  ms. Soon after this somewhat superficial episode of convective overturn, a PNS suffers from deep convective instability for the duration of the Kelvin-Helmholtz time (Thompson & Murray 2001, hereafter TM01; Burrows & Lattimer 1986 Burrows 1987; TD93; Keil, Janka, & Mueller 1996, hereafter KJM96; Pons et al. 1999). KJM96 find that Ledoux-type convection quickly recedes from the neutrinosphere in  $\sim 20$ – $30$  ms, moving deep into the core and at about  $\sim 1$ s after bounce, the entire star is convective. TD93 point out that in PNSs, the ratio of convective kinetic energy to gravitational binding energy  $\sim 100$  times larger than its progenitor during the Silicon burning phase and  $\sim 10^3$ – $10^4$  times larger when the progenitor resided on the main sequence. In fact, when compared this way, convection in PNSs is  $\sim 10^4$  times more violent than the Sun. Primarily motivated by this fact, TD93 conclude that PNSs are efficient sites of dynamo activity.

The theory of magnetic field generation and its subsequent evolution in young PNSs is primarily put forth by TD93 and then further elaborated by TM01. A summary of their findings, relevant for this work, is given below.

### 2.1.1. Case of Rapid Rotation–Magnetars

Based on theoretical and phenomenological arguments, Duncan and Thompson (1992) and TD93 conclude that PNSs with initial rotation periods near break up ( $P_{\text{rot}} \sim 1$  ms) efficiently convert the nascent star’s rotational shear energy into toroidal and poloidal flux via  $\alpha$ – $\Omega$  dynamo action at the base of the convection zone where the overturn time is similarly  $\sim 1$  ms. They argue that the free energy available from differential rotation  $E_{\Omega}$  for rapidly rotating ( $P_{\text{rot}} \sim 1$  ms) PNSs is roughly  $E_{\Omega} \sim 10^{52}$  ergs. This enormous reservoir of energy could in principle, generate ordered fields as strong as  $B \sim 3 \times 10^{17}$  G throughout the star. This led them to conclude that PNSs born rotating near break up form dipole fields during the convective Kelvin-Helmholtz phase that are much stronger than those of pulsars. These highly magnetized neutron stars with dipole field strengths  $B_{\text{dip}} \sim 10^{14}$ – $10^{15}$  G are referred to as “magnetars.”

### 2.1.2. Slow Rotation – Analogy with the Solar Convection Zone

In the absence of rapid rotation or a large reservoir of helicity, turbulent convection alone may lead to sizable magnetic stresses. There is some phenomenological evidence for this idea, most of which comes from the Sun. Between 1986 and 1988, a period of increasing solar magnetic activity, the solar 5-minute acoustic oscillations displayed a significant (one part in  $10^4$ ) increase in frequency (Libbrecht & Woodard 1990). A rise in the rms magnetic stress to values of  $B_{\text{rms}} \sim 200$  G at the top of the convection zone, and extending downwards to substantial depth with greater strength, could explain the observed trend in acoustic frequency (Goldreich et. al 1991). At the top of the solar convection zone, the overturn time ( $\sim 5$ – $10$  min) is much shorter than the rotation period ( $\sim 22$  days). Therefore, it seems that convective motions alone may sustain near equipartition (with the turbulence) rms fields on timescales that are many orders of magnitude in excess of the convective overturn time.

In PNSs, unlike the solar convection zone, the gradient of the turbulent diffusivity lies in the opposite direction with respect to the buoyancy force acting on a given flux rope in thermal equilibrium with its surrounding (Tobias et. al 1998, 2001; TM01). As a result, both buoyancy and turbulent diffusion tend to transport magnetic structures of scale  $l_p$ , the gas pressure scale height, to the top of the convection zone approximately in an overturn time.<sup>6</sup> At the same time, flux ropes that are generated and amplified by the stretching action of the convective cells are pinned at the base of the overshoot region.

One of the most commonly held beliefs in dynamo theory is that turbulent magnetic fields generated and amplified by convective overturn come roughly into equipartition with the turbulent kinetic energy. Mixing length theory provides for a rough estimate of the convective velocities at the base of the convection zone

$$F_c \sim \rho v_c^3 \longrightarrow v_c \sim 2 \times 10^8 F_{39}^{1/3} \rho_{14}^{-1/3} \text{ cms}^{-1} \quad (2)$$

where  $F_c$  and  $v_c$  are the convective energy flux and velocity amplitude, respectively. This yields a saturation field strength

$$B_{\text{sat}} \sim \sqrt{4\pi\rho v_c} \sim 6 \times 10^{15} F_{39}^{1/3} \rho_{14}^{1/6} \text{ G} \quad (3)$$

on the scale of a pressure scale height  $l_p$  at the base of the convection zone where  $l_p \sim 1$ – $10$  km. If a near-equipartition magnetic flux tube generated at the the base of the convection zone is “pumped” and pinned to the top of the PNS convection zone in the overshoot region (KJM96, TM01), then the local field strength may approach equipartition *with the matter* near the neutrinosphere for typical values of temperature and density ( $T_{\nu} \sim$  a few MeV and  $\rho_{\nu} \lesssim 10^{12} \text{ g cm}^{-3}$ ) at relatively small depths.

### 2.1.3. Long-Lived Large Scale Magnetic Structures in the Limit of Slow Rotation

The ratio of the length scale of the energy bearing eddies to the radius of the neutrinosphere,  $l_p/R_{\nu} \sim 10^{-1}$ , is  $\sim 10^3$  times larger than the analogous ratio for the Sun. This leads one to believe that the magnetic structures that are produced by convective turbulence in PNSs are much larger than those of the Sun as a fraction of the total stellar radius (TD93). The value of the fluctuating rms magnetic field is given by

$$B_{\text{rms}} \sim \epsilon_B^{1/2} B_{\text{sat}}, \quad (4)$$

where  $\epsilon_B$  is the convective efficiency parameter. In the Sun,  $\epsilon_B \sim 0.1$  (Goldreich et al. 1991) and if we naively extrapolate this value to PNSs, we obtain with the help of eq. (3) and with all things being equal,  $B_{\text{rms}} \sim 2 \times 10^{15}$ . One suspects that these magnetic structures,

<sup>6</sup> This is true so long as magnetic flux is *passively* mixed by the turbulence.



with spatial dimension roughly equal to the depth of the radiative layer above the convection zone, are created and destroyed on the eddy turnover time  $\sim 1$ ms. However, Cattaneo and Vainshtein (1991) point out that larger scale structures with smaller flux densities can effectively resist eddy diffusivity for a significant number of overturns, implying a breakdown of kinetic approximation. If a starspot possesses a dimension  $l_{\text{spot}} \sim 3l_p$  and is due to the random orientation of the smaller dipoles created on the scale of the energy bearing eddies, its field strength  $B_{\text{spot}} \sim 1/10B_{\text{rms}} \sim 2(\epsilon_B/0.1)^{1/2} \times 10^{14}$  G. Such a starspot covers  $\sim$  a few % of the surface of the PNS and may exist for several hundred turnover times before eddy diffusivity can efficiently transfer flux from large scale structures to the eddy scale (Cattaneo & Vainshtein 1991).

From an even more phenomenological perspective, supergranulation on the surface of the Sun may provide a clue to the mechanism of large scale field generation in slowly rotating PNSs. In the Sun's quiet photospheric network, magnetic flux is generated and destroyed by granule and supergranule motions, rather than originating from the strongly magnetized active regions (Schrijver et al. 1997). The intermittent magnetic fields associated with supergranule motion typically approach equipartition with the supergranule flow while lasting only a few supergranule lifetimes.

The characteristic scale of a solar supergranule is  $\sim 30$  times larger than the gas pressure scale height at the photosphere or equivalently,  $\sim 30$  times larger than a characteristic granule (Stenflo 1989). Also, supergranules overturn with velocities that are  $\sim$  a few times slower than the velocities associated with granular motion, which are  $\sim 1 \text{ km s}^{-1}$  in the Sun. If we savagely map the solar values for granule and supergranule motion to the surfaces of PNSs, one expects supergranule lifetimes on the surface of the PNSs to be anywhere from a few hundreds of milliseconds to a few seconds. The scale height of the neutrinosphere  $\sim 1/30$  the stellar radius measured at the neutrinosphere  $R_\nu$ , implying that only a single supergranule may encompass a sizable fraction of a PNS.

So far, we have provided the impetus for studying neutrino bubble instabilities in PNSs by motivating the existence of a small number of strongly magnetized starspots. Now, we consider in detail the local dynamics and thermodynamics of their linear driving mechanism. The next few sections are quite technical. They are riddled with large algebraic expressions whose meanings may not be immediately transparent to the untrained eye. For readers not concerned with the details of linear radiation magnetohydrodynamics in degenerate media, we suggest skipping ahead to §5.6 where estimates of stability and driving are given in terms of physical parameters appropriate for PNSs.

### 3. FUNDAMENTAL ASSUMPTIONS AND EQUILIBRIUM

We consider fluid perturbations upon a highly conducting magnetized fluid consisting of neutrons, protons, electrons, and photons interacting with radiation consisting of neutrinos (and anti-neutrinos) of all flavors. The interaction between normal matter and the neutrinos is mediated by the various sources of opacity. We make the simplifying assumption that all neutrino opacities increase with the square of the neutrino energy  $E$ . In particular, for electron neutrinos and anti-neutrinos,

$$\kappa_{\nu_e, \bar{\nu}_e} = \kappa_0 \left( \frac{E}{E_0} \right)^2, \quad (5)$$

whereas for all other types of neutrinos,

$$\kappa_{\nu_X} = \kappa_{0X} \left( \frac{E}{E_0} \right)^2. \quad (6)$$

(We adopt the same constant fiducial energy scale  $E_0$  in both cases.) The prefactors  $\kappa_0$  and  $\kappa_{0X}$  are assumed to be constant and independent of composition. Only the electron-type neutrinos can be absorbed and emitted by pair capture processes

$$\begin{aligned} e^- + p &\rightleftharpoons n + \nu_e \\ e^+ + n &\rightleftharpoons p + \bar{\nu}_e \end{aligned} \quad (7)$$

implying that only the electron-type neutrinos can exchange energy with the matter while all neutrinos can exchange momentum with the matter via elastic neutrino-nucleon scattering

$$\nu + N \rightleftharpoons \nu + N \quad (8)$$

where  $\nu$  represents any of the six ( $\nu_e, \bar{\nu}_e, \nu_X, \bar{\nu}_X$ ) neutrino species and  $N$  denotes either neutrons or protons.

For now, we shall assume that thermal equilibrium

$$T_g = T_\nu, \quad (9)$$

where  $T_g$  is the gas temperature of the gas, and chemical equilibrium

$$\mu_p + \mu_e = \mu_n + \mu_{\nu_e}, \quad (10)$$

where  $\mu_i$  is the chemical potential of the  $i^{\text{th}}$  species, hold in both the equilibrium *and* the perturbed state<sup>7</sup>. This assertion is more subtle than it appears at first glance and we discuss its accuracy later on in this work.

Assuming that the neutrinos are optically thick and that the neutron-proton-electron-photons ( $npe\gamma$ ) fluid is an excellent conductor, the expressions for mass, momentum, lepton fraction, energy, and magnetic flux conservation are

$$\frac{\partial \rho}{\partial t} + \nabla \cdot (\rho \mathbf{v}) = 0, \quad (11)$$

<sup>7</sup> At temperature and densities typical for young PNSs, strong and electromagnetic interactions easily maintain thermal balance between baryons, electrons, and photons. Also since these species are so well coupled to one another, their mean free paths are vanishingly small. For these reasons, from here on we shall refer to "the fluid" or "the gas" as the multi-species gas consisting of neutrons, protons, electrons, and photons.

$$\rho \left( \frac{\partial \mathbf{v}}{\partial t} + \mathbf{v} \cdot \nabla \mathbf{v} \right) = -\nabla P + \rho \mathbf{g} + \frac{1}{4\pi} (\nabla \times \mathbf{B}) \times \mathbf{B}, \quad (12)$$

$$n \left( \frac{\partial Y_L}{\partial t} + \mathbf{v} \cdot \nabla Y_L \right) = -\nabla \cdot \mathbf{F}_L, \quad (13)$$

$$\frac{\partial U}{\partial t} + \mathbf{v} \cdot \nabla U + (U + P) \nabla \cdot \mathbf{v} = -\nabla \cdot \mathbf{F}, \quad (14)$$

$$\frac{\partial \mathbf{B}}{\partial t} = \nabla \times (\mathbf{v} \times \mathbf{B}), \quad (15)$$

and

$$\nabla \cdot \mathbf{B} = 0 \quad (16)$$

respectively. Here,  $\rho$ ,  $\mathbf{v}$ ,  $P$ ,  $\mathbf{g}$ ,  $\mathbf{B}$ ,  $U$ ,  $\mathbf{F}$ ,  $Y_L$ , and  $\mathbf{F}_L$  are the fluid density, fluid momentum, total ( $npe\gamma$ +neutrinos) pressure, local tidal gravitational field, the magnetic field, total energy density, neutrino flux, lepton fraction, and lepton flux, respectively.

Since PNSs are optically thick to neutrinos of all types, we assume that in eqs. (12), (13), and (14) the diffusion approximation accurately describes energy and lepton transport as well as momentum exchange. Thus, we only consider fluid perturbations that are optically thick to neutrino diffusion, restricting our analysis to the region below the surface of last scattering i.e., below the neutrinosphere. The radiative energy flux  $\mathbf{F}$  is given by the sum

$$\mathbf{F} = \mathbf{F}_{\nu_e} + \mathbf{F}_{\bar{\nu}_e} + \mathbf{F}_{\nu_X} \quad (17)$$

where  $\mathbf{F}_i$  is the energy flux of the  $i^{\text{th}}$  species. The energy flux for electron-type and  $X$ -type neutrinos is given by

$$\mathbf{F}_{\nu_e} + \mathbf{F}_{\bar{\nu}_e} = -\frac{E_0^2 k_B^2}{6\pi^2 \kappa_0 \rho \hbar^3 c^2} \nabla \left( \frac{T^2 \eta_{\nu_e}^2}{2} + \frac{\pi^2}{6} T^2 \right) \quad (18)$$

and

$$\mathbf{F}_{\nu_X} = -\frac{E_0^2 k_B^2}{18\kappa_{0X} \rho \hbar^3 c^2} \nabla T^2, \quad (19)$$

respectively. Since  $X$ -type neutrinos are created in the neutral current pair annihilation process, an excess of  $\mu$ - or  $\tau$ -type neutrinos is absent. As a result, only electron-type neutrinos carry lepton number due to their ability of being absorbed and emitted during pair capture and emission processes. The lepton flux is given by

$$\mathbf{F}_L = -\frac{E_0^2 k_B}{6\pi^2 \kappa_0 \rho \hbar^3 c^2} \nabla (T \eta_{\nu_e}). \quad (20)$$

The expressions for neutrino energy and lepton fluxes as well as other important thermodynamic quantities obtained from Fermi-Dirac distributions are briefly derived in Appendix A. The degeneracy parameter  $\eta_i = \mu_i / k_B T$  will be interchanged with  $\mu_i$  throughout this work depending on the particular application involved. The mass density is given in terms of the nucleon or baryon number density

$$\rho = n m_n, \quad (21)$$

where  $m_n$  is the mass of the neutron, implying that the mass difference between the neutron and proton has been ignored when evaluating the density. The total pressure and energy density are given by

$$P = \frac{1}{3} (U_{e^-} + U_{e^+} + U_\gamma + U_{\nu_e} + U_{\bar{\nu}_e} + U_{\nu_X}) + \frac{2}{3} U_b \quad (22)$$

and

$$U = U_{e^-} + U_{e^+} + U_\gamma + U_{\nu_e} + U_{\bar{\nu}_e} + U_{\nu_X} + U_b \quad (23)$$

where

$$U_b = U_b(\rho, T, Y_p, Y_n), \quad (24)$$

$$U_{e^-} + U_{e^+} = \frac{7\pi^2 k_B^4 T^4}{60\hbar^3 c^3} \left[ 1 + \frac{30}{7} \left( \frac{\eta_e}{\pi} \right)^2 + \frac{15}{7} \left( \frac{\eta_e}{\pi} \right)^4 \right], \quad (25)$$

$$U_\gamma = \frac{\pi^2 k_B^4 T^4}{15\hbar^3 c^3} = a T^4, \quad (26)$$

$$U_{\nu_e} + U_{\bar{\nu}_e} = \frac{7\pi^2 k_B^4 T^4}{120\hbar^3 c^3} \left[ 1 + \frac{30}{7} \left( \frac{\eta_{\nu_e}}{\pi} \right)^2 + \frac{15}{7} \left( \frac{\eta_{\nu_e}}{\pi} \right)^4 \right], \quad (27)$$

$$\text{and } U_{\nu_X} + U_{\bar{\nu}_X} = 4 \times \frac{7}{8} a T^4. \quad (28)$$

The electron and electron neutrino fractions are given by

$$Y_e = \frac{n_{e^-} - n_{e^+}}{n} = \frac{k_B^3 T^3}{3n\hbar^3 c^3} \eta_e \left( 1 + \frac{\eta_e^2}{\pi^2} \right) \quad \text{and} \quad Y_{\nu_e} = \frac{n_{\nu_e} - n_{\bar{\nu}_e}}{n} = \frac{k_B^3 T^3}{6n\hbar^3 c^3} \eta_{\nu_e} \left( 1 + \frac{\eta_{\nu_e}^2}{\pi^2} \right), \quad (29)$$

where the total lepton fraction is defined as  $Y_L = Y_e + Y_{\nu_e}$ . The baryon energy density,  $U_b$ , is given by that of a monatomic ideal gas near the neutrinosphere, where the effects of degeneracy pressure are negligible for the baryons. However, in the core the zero-point Fermi pressure is substantial for the baryons, which is why we have written the baryon equation of state in a somewhat general manner since its form depends on the location below the neutrinosphere.

The condition for chemical equilibrium may be written as

$$\frac{(m_n - m_p)c^2}{k_B T} - \ln \left[ \left( \frac{m_n}{m_p} \right)^{3/2} \left( \frac{Y_p}{Y_n} \right) \right] = \eta_e - \eta_{\nu_e} \quad (30)$$

and the fact that the total nucleon number density  $n$  is conserved implies

$$Y_p + Y_n = 1. \quad (31)$$

Finally, charge neutrality implies

$$Y_p = Y_e = \frac{k_B^3 T^3}{3n\hbar^3 c^3} \eta_e \left( 1 + \frac{\eta_e^2}{\pi^2} \right). \quad (32)$$

This gives us 21 equations for 21 variables:  $\rho$ ,  $\mathbf{v}$ ,  $P$ ,  $\mathbf{B}$ ,  $U$ ,  $\mathbf{F}$ ,  $n$ ,  $Y_L$ ,  $T$ ,  $\eta_e$ ,  $\eta_{\nu_e}$ ,  $Y_p$ ,  $Y_n$ ,  $(\mathbf{F}_{\nu_e} + \mathbf{F}_{\bar{\nu}_e})$ ,  $\mathbf{F}_{\nu_x}$ ,  $\mathbf{F}_L$ ,  $U_b$ ,  $(U_{e^-} + U_{e^+})$ ,  $U_\gamma$ ,  $(U_{\nu_e} + U_{\bar{\nu}_e})$ , and  $U_{\nu_x}$ .

We treat the background state of the PNS envelope in a fashion similar to that of a normal main sequence star. The gravitational field is assumed to be fixed, which is a good approximation for our oscillation wavelengths of interest near the neutrinosphere, where the radiative flux is roughly constant with depth as well. That is, we adopt a plane parallel approximation. Rather than photons transporting energy from one depth to the next, neutrinos of all flavors take on that role. Also, we implicitly assume that chemical and thermal equilibrium holds for our static background and perturbations. For PNSs, this condition is met for any dynamical timescale of interest below the neutrinosphere (see Appendix C for a detailed discussion regarding chemical and thermal equilibrium).

The major qualitative difference between the environments of PNSs and the stellar envelopes considered by Blaes & Socrates (2003) is that the radiation considered here is degenerate with a large chemical potential. Since the flow is optically thick, gradients in both neutrino temperature and chemical potential transport both neutrino energy (not just heat) and particle number. For the black body ( $\mu = 0$ ) radiation fields considered by Blaes & Socrates (2003), the background radiation flux interacts with short-wavelength compressible fluid perturbations in two ways. Radiation piles up downstream density maxima with respect to the background flux  $\mathbf{F}$ , an effect known as ‘‘shadowing’’ (Lucy & White 1980, Lucy 1982). Thus, the radiation flux couples to the density perturbation, producing a pressure response  $\propto \mathbf{F} \cdot \nabla \delta \rho$ . The other effect arises from changes in a fluid element’s position during oscillation with respect to surfaces of constant background radiation pressure, which results in a pressure response  $\propto \boldsymbol{\xi} \cdot \mathbf{F}$  where  $\boldsymbol{\xi}$  is the fluid displacement. In the case of PNSs, both  $\mathbf{F}$  and  $\mathbf{F}_L$  interact with compressible short wave-length fluid oscillations in this manner. Therefore, neutrino bubble instabilities are driven by both  $\mathbf{F}$  and  $\mathbf{F}_L$  rather than just  $\mathbf{F}$  alone. More fundamentally, radiative diffusion due to gradients in both temperature and chemical potential are responsible for radiative driving, but otherwise the mechanics of photon bubble-like instability is the same as the neutrino bubble instability.

#### 4. TOTAL PRESSURE PERTURBATION IN THE LIMIT OF RAPID NEUTRINO DIFFUSION

We wish to study standard magnetosonic motion altered by the presence of radiative diffusion. In the optically thick limit, radiation alters the fluid’s motion by gradients in its pressure. The instabilities classified by Blaes & Socrates (2003) occur in the limit where radiation diffuses rapidly compared to the local magnetoacoustic crossing time. We consider the same limit here.

Generally speaking, the total pressure may be written as

$$P = P(\rho, T, \mu_e, \mu_{\nu_e}) \quad (33)$$

and upon perturbation, we have

$$\delta P = \delta \rho \left( \frac{\partial P}{\partial \rho} \right)_{T, \mu_e, \mu_{\nu_e}} + \delta T \left( \frac{\partial P}{\partial T} \right)_{\rho, \mu_e, \mu_{\nu_e}} + \delta \mu_e \left( \frac{\partial P}{\partial \mu_e} \right)_{\rho, T, \mu_{\nu_e}} + \delta \mu_{\nu_e} \left( \frac{\partial P}{\partial \mu_{\nu_e}} \right)_{\rho, T, \mu_e}. \quad (34)$$

We may eliminate  $\mu_e$  in terms of  $\rho, T$ , and  $\mu_{\nu_e}$  by use of the eqs. (30), (31), and (32) which denote beta equilibrium, baryon conservation, and charge conservation, respectively. The total pressure perturbation may then be written as

$$\delta P = \delta \rho \left( \frac{\partial P}{\partial \rho} \right)_{T, \mu_{\nu_e}} + \delta T \left( \frac{\partial P}{\partial T} \right)_{\rho, \mu_{\nu_e}} + \delta \mu_{\nu_e} \left( \frac{\partial P}{\partial \mu_{\nu_e}} \right)_{\rho, T}. \quad (35)$$

As previously mentioned, neutrinos diffuse down gradients of both temperature and neutrino chemical potential. In the limit of rapid diffusion, the spatial distribution and relative amplitude of the neutrino temperature and chemical potential are almost purely determined by the divergence of the neutrino and lepton flux. To see this clearly, we write the linearized expressions for conservation of lepton number, eq. (13), and the first law of thermodynamics, eq. (14). This gives us

$$-i\omega \delta Y_L + \delta \mathbf{v} \cdot \nabla Y_L = -i\omega \left[ \left( \frac{\partial Y_L}{\partial T} \right)_{\rho, \mu_{\nu_e}} \delta T + \left( \frac{\partial Y_L}{\partial \mu_{\nu_e}} \right)_{\rho, T} \delta \mu_{\nu_e} + \left( \frac{\partial Y_L}{\partial \rho} \right)_{T, \mu_{\nu_e}} \delta \rho \right] + \delta \mathbf{v} \cdot \nabla Y_L = -\frac{i}{n} \mathbf{k} \cdot \delta \mathbf{F}_L \quad (36)$$

$$-i\omega \delta U + \delta \mathbf{v} \cdot \nabla U + i(U + P) \mathbf{k} \cdot \delta \mathbf{v} = -i\omega \left[ \left( \frac{\partial U}{\partial T} \right)_{\rho, \mu_{\nu_e}} \delta T + \left( \frac{\partial U}{\partial \mu_{\nu_e}} \right)_{\rho, T} \delta \mu_{\nu_e} + \left( \frac{\partial U}{\partial \rho} \right)_{T, \mu_{\nu_e}} \delta \rho \right] + \delta \mathbf{v} \cdot \nabla U + i(U + P) \mathbf{k} \cdot \delta \mathbf{v} = -i \mathbf{k} \cdot \delta \mathbf{F}. \quad (37)$$

$\delta \mathbf{F}_L$  and  $\delta \mathbf{F}$  are given by

$$\delta \mathbf{F}_L = -\frac{\delta \rho}{\rho} \mathbf{F}_L - \frac{i\mathcal{K}}{\pi^2 \kappa_0 \rho} \mathbf{k} \delta \mu_{\nu_e} \quad (38)$$

and

$$\delta \mathbf{F} = -\frac{\delta \rho}{\rho} \mathbf{F} - \frac{i\mathcal{K}k_B^2 T}{\kappa_{\text{eff}} \rho} \mathbf{k} \delta T - \frac{i\mathcal{K}\mu_{\nu_e}}{\pi^2 \kappa_0 \rho} \mathbf{k} \delta \mu_{\nu_e} \quad (39)$$

where

$$\mathcal{K} \equiv \frac{E_0^2}{6\hbar^3 c^2} \quad \text{and} \quad \frac{1}{\kappa_{\text{eff}}} \equiv \frac{2}{3\kappa_{0X}} + \frac{1}{3\kappa_0}. \quad (40)$$

Note that we are operating within the framework of the WKB approximation where all perturbation quantities take on a plane wave-like form  $\propto e^{i(\mathbf{k}\cdot\mathbf{x}-\omega t)}$ . Therefore, our analysis from here on, is only credible for perturbations with wavelengths smaller than the gas pressure scale height.

From eq. (38), the change in lepton flux is determined by gradients in the neutrino chemical potential mediated by the electron neutrino opacity as well as a component that arises from changes in density. Eq. (39) implies that changes in the radiative heat flux originate from both changes in the temperature gradient mediated by the sum of the electron- and  $X$ -type neutrino opacities and gradients in the neutrino chemical potential mediated solely by the electron neutrino opacity in addition to a component that comes from fluctuations in density.

A first step in obtaining the total pressure perturbation is to solve for  $\delta \mu_{\nu_e}$  in terms of the other thermodynamic variables,  $\delta T$  and  $\delta \rho$ . We (arbitrarily) choose the linearized expression for lepton conservation, eq. (36) as our starting point. We have,

$$-in\omega \left[ \left( \frac{\partial Y_L}{\partial T} \right)_{\mu_{\nu_e}, \rho} \delta T + \left( \frac{\partial Y_L}{\partial \mu_{\nu_e}} \right)_{T, \rho} \delta \mu_{\nu_e} + \left( \frac{\partial Y_L}{\partial \rho} \right)_{T, \mu_{\nu_e}} \delta \rho \right] + n \delta \mathbf{v} \cdot \nabla Y_L = i \frac{\delta \rho}{\rho} \mathbf{k} \cdot \mathbf{F}_L - \frac{k^2 \mathcal{K}}{\pi^2 \kappa_0 \rho} \delta \mu_{\nu_e}. \quad (41)$$

It is useful to define a characteristic diffusion frequency,  $\omega_{L, \text{diff}}$  associated with  $Y_L$  transport

$$\omega_{L, \text{diff}} \equiv \omega + i \frac{k^2 \mathcal{K}}{\pi^2 \kappa_0 \rho n \left( \frac{\partial Y_L}{\partial \mu_{\nu_e}} \right)_{\rho, T}}, \quad (42)$$

which allows us to write

$$\delta \mu_{\nu_e} = -\frac{\omega}{\omega_{L, \text{diff}}} \frac{\left( \frac{\partial Y_L}{\partial \rho} \right)_{T, \mu_{\nu_e}}}{\left( \frac{\partial Y_L}{\partial \mu_{\nu_e}} \right)_{\rho, T}} \delta \rho - \frac{\mathbf{k} \cdot \mathbf{F}_L}{n \omega_{L, \text{diff}} \left( \frac{\partial Y_L}{\partial \mu_{\nu_e}} \right)_{\rho, T}} \frac{\delta \rho}{\rho} - \frac{\omega}{\omega_{L, \text{diff}}} \frac{\left( \frac{\partial Y_L}{\partial T} \right)_{\rho, \mu_{\nu_e}}}{\left( \frac{\partial Y_L}{\partial \mu_{\nu_e}} \right)_{\rho, T}} \delta T - i \frac{\delta \mathbf{v} \cdot \nabla Y_L}{\omega_{L, \text{diff}} \left( \frac{\partial Y_L}{\partial \mu_{\nu_e}} \right)_{\rho, T}}. \quad (43)$$

BS03 found that in the limit of rapid radiative diffusion, temperature perturbations become reduced on the scale of the mode wavelength as long as the characteristic diffusion timescale is much shorter than the mode's period. Here, both the temperature and neutrino chemical potential are subject to the same diffusive reduction since neutrino diffusion occurs along gradients of both temperature and chemical potential. Following BS03, we recognize that in the rapidly diffusing limit,

$$\delta \mu_{\nu_e}, \delta T \propto \frac{\omega}{\omega_{\text{diff}}} \delta \rho \propto k^{-1} \delta \rho \quad (44)$$

where  $\omega_{\text{diff}}$  represents some characteristic diffusion frequency. Note that we have assumed that  $\omega \propto k$ , which implies that we are investigating the properties of short-wavelength MHD waves i.e., the Alfvén, fast, and slow waves. Many authors have noted that in general, there are two diffusion frequencies associated for both lepton and energy transport in optically thick PNSs (Bruenn & Dineva 1996, Pons et al. 1999, Miralles et al. 2000, Bruenn, Raley, & Mezzacappa 2004). That is, lepton and energy diffusion together evolve down gradients of both lepton fraction and entropy (or alternatively, temperature and neutrino chemical potential). Rather than investigating overturn instability phenomena such as Ledoux convection, “neutron-fingers,” and semi-convection, we focus on questions of acoustic stability in the limit where sound waves (and magnetosonic waves) are highly non-adiabatic. That is, both lepton and energy diffusion occur rapidly in comparison to the acoustic crossing time of interest for a given oscillation wavelength. Due to our  $\propto E^2$  opacity parameterization, the “cross-term” for lepton diffusion is absent, constraining lepton evolution to depend only on gradients in neutrino chemical potential denoted, here by a single diffusion frequency  $\omega_{L, \text{diff}}$ .

Now, in the short-wavelength high- $k$  rapidly diffusing limit, the characteristic frequency associated with lepton diffusion satisfies

$$|\omega_{L, \text{diff}}| \rightarrow \frac{k^2 \mathcal{K}}{\pi^2 \kappa_0 \rho n \left( \frac{\partial Y_L}{\partial \mu_{\nu_e}} \right)_{\rho, T}} \gg \omega. \quad (45)$$

With this, the neutrino chemical potential is approximately given by

$$\delta \mu_{\nu_e} \simeq i \frac{\pi^2 \kappa_0 \rho}{k^2 \mathcal{K}} \times \left[ n \omega \left( \frac{\partial Y_L}{\partial \rho} \right)_{T, \mu_{\nu_e}} + \frac{\mathbf{k} \cdot \mathbf{F}_L}{\rho} \right] \delta \rho. \quad (46)$$

The first term on the right hand side produces damping in much the same way as classical Silk damping (Silk, 1968). There are however, some subtleties to this concept – a point we will consider later on. The second term  $\propto \mathbf{k} \cdot \mathbf{F}_L$  is in part, responsible for driving arising from the background *lepton* flux interacting with changes in the fluid's density. Note that we have made use of the fact that  $|\delta \mathbf{v}| \propto \delta \rho$  for acoustic and magnetosonic waves, which allowed us to drop the term in eq. (43)  $\propto \delta \mathbf{v} \cdot \nabla Y_L$ .



In order to calculate  $\delta T$  in terms of  $\delta\rho$ , we perform the analysis for rapid diffusion with respect to the first law of thermodynamics. We have

$$\begin{aligned} -i\omega \left\{ \left( \frac{\partial U}{\partial T} \right)_{\mu\nu_e, \rho} \delta T + \left( \frac{\partial U}{\partial \mu\nu_e} \right)_{T, \rho} \delta\mu\nu_e + \left[ \left( \frac{\partial U}{\partial \rho} \right)_{T, \mu\nu_e} - \frac{U+P}{\rho} \right] \delta\rho \right\} + \delta\mathbf{v} \cdot [\nabla U - (U+P)\nabla \ln\rho] \\ = i\mathbf{k} \cdot \mathbf{F} \frac{\delta\rho}{\rho} - k^2 \frac{\mathcal{K}k_B^2 T}{\kappa_{\text{eff}}\rho} \delta T - k^2 \frac{\mathcal{K}\mu\nu_e}{\pi^2 \kappa_0 \rho} \delta\mu\nu_e. \end{aligned} \quad (47)$$

Now, we may define another characteristic neutrino diffusion frequency,  $\omega_{\text{E,diff}}$  which measures the relative importance of energy transport via the diffusion of neutrinos down their temperature gradient

$$\omega_{\text{E,diff}} \equiv \omega + i \frac{k^2 \mathcal{K} k_B^2 T}{\kappa_{\text{eff}} \rho (\partial U / \partial T)_{\rho, \mu\nu_e}}. \quad (48)$$

In a similar fashion to  $\delta\mu\nu_e$ , the temperature perturbation becomes

$$\begin{aligned} \delta T = -\frac{\omega}{\omega_{\text{E,diff}}} \frac{(\partial U / \partial \mu\nu_e)_{\rho, T}}{(\partial U / \partial T)_{\rho, \mu\nu_e}} \delta\mu\nu_e - \frac{\omega}{\omega_{\text{E,diff}}} \frac{(\partial U / \partial \rho)_{T, \mu\nu_e} - (U+P)/\rho}{(\partial U / \partial T)_{\rho, \mu\nu_e}} \delta\rho - i \frac{\delta\mathbf{v} \cdot [\nabla U - (U+P)\nabla \ln\rho]}{\omega_{\text{E,diff}} (\partial U / \partial T)_{\rho, \mu\nu_e}} \\ - \frac{\mathbf{k} \cdot \mathbf{F}}{\omega_{\text{E,diff}} (\partial U / \partial T)_{\rho, \mu\nu_e}} \frac{\delta\rho}{\rho} - i \frac{k^2 \mathcal{K} \mu\nu_e}{\pi^2 \kappa_0 \rho \omega_{\text{E,diff}} (\partial U / \partial T)_{\rho, \mu\nu_e}} \delta\mu\nu_e. \end{aligned} \quad (49)$$

In the short-wavelength high- $k$  limit, energy transport by means of neutrino diffusion is rapid compared to the acoustic or magnetoacoustic crossing time such that

$$|\omega_{\text{E,diff}}| \rightarrow \frac{k^2 \mathcal{K} k_B^2 T}{\kappa_{\text{eff}} \rho (\partial U / \partial T)_{\rho, \mu\nu_e}} \gg \omega. \quad (50)$$

Again, by realizing that  $\delta\mu\nu_e \propto k^{-1}\delta\rho$  and  $|\delta\mathbf{v}| \propto \delta\rho$  for acoustic and magnetosonic waves in short-wavelength limit, the temperature perturbation may be written as

$$\delta T \simeq i \frac{\kappa_{\text{eff}}\rho}{k^2 \mathcal{K} k_B^2 T} \times \left\{ \omega \left[ \left( \frac{\partial U}{\partial \rho} \right)_{T, \mu\nu_e} - \frac{U+P}{\rho} \right] \delta\rho + \frac{\mathbf{k} \cdot \mathbf{F}}{\rho} \delta\rho + i \frac{k^2 \mathcal{K} \mu\nu_e}{\pi^2 \kappa_0 \rho} \delta\mu\nu_e \right\}, \quad (51)$$

and with the help of eq. (46), we have

$$\delta T \simeq i \frac{\kappa_{\text{eff}}\rho}{k^2 \mathcal{K} k_B^2 T} \times \left\{ \omega \left[ \left( \frac{\partial U}{\partial \rho} \right)_{T, \mu\nu_e} - \frac{U+P}{\rho} - \mu\nu_e n \left( \frac{\partial Y_L}{\partial \rho} \right)_{T, \mu\nu_e} \right] + \frac{\mathbf{k} \cdot [\mathbf{F} - \mu\nu_e \mathbf{F}_L]}{\rho} \right\} \delta\rho. \quad (52)$$

The first three terms inside the braces in eq. (52) represent Silk damping. Upon compression, neutrinos leak out along the temperature gradient of the fluid element and cool the gas. Cooling during compression can be thought of as a general criterion for damping. The term  $\propto [\mathbf{F} - \mu\nu_e \mathbf{F}_L]$  is responsible for unstable driving due to a combination of both the energy and lepton flux coupling to fluctuations in density.

In this light, the total pressure perturbation is divided into two parts; one which yields a standard acoustic response  $\propto \delta\rho$  while the other component  $\propto ik^{-1}\delta\rho$  leads to radiative driving and damping. That is,

$$\delta P = \delta P_{\text{ac}} + \delta \tilde{P} \quad (53)$$

where

$$\delta P_{\text{ac}} = \left( \frac{\partial P}{\partial \rho} \right)_{T, \mu\nu_e} \delta\rho \quad \text{and} \quad \delta \tilde{P} = \left( \frac{\partial P}{\partial T} \right)_{\rho, \mu\nu_e} \delta T + \left( \frac{\partial P}{\partial \mu\nu_e} \right)_{\rho, T} \delta\mu\nu_e. \quad (54)$$

The quantity

$$\left( \frac{\partial P}{\partial \rho} \right)_{T, \mu\nu_e} = \left( \frac{\partial P}{\partial \rho} \right)_{T, \mu\nu_e, \mu_e} + \left( \frac{\partial \mu_e}{\partial \rho} \right)_{T, \mu\nu_e} \left( \frac{\partial P}{\partial \mu_e} \right)_{\rho, T, \mu\nu_e} \equiv c_i^2 \quad (55)$$

is the square of the isothermal and ‘‘isomeric’’ sound speed  $c_i$ .<sup>8</sup> When pair capture and emission occur prodigiously, the rapid exchange of electron-type neutrinos fixes the gas temperature to that of the neutrinos and the composition of the  $npe\gamma$  gas is determined by the evolution of the electron-type neutrino’s chemical potential. Due to rapid neutrino diffusion, which depends on the gradients of both the neutrino temperature and chemical potential, perturbations in temperature and neutrino chemical potential are smaller by a factor  $\propto k^{-1}$  in the short-wavelength limit. Upon compression, both the temperature and relative chemical composition of a given fluid element remain fixed to lowest  $\mathcal{O}(k^{-1})$  while its density and electron chemical potential evolve. With this in mind, by combining eqs. (35), (46), and (52) the total pressure perturbation may be written as

$$\begin{aligned} \delta P = c_i^2 \delta\rho + i \left( \frac{\partial P}{\partial T} \right)_{\rho, \mu\nu_e} \frac{\kappa_{\text{eff}}\rho}{k^2 \mathcal{K} k_B^2 T} \times \left\{ \omega \left[ \left( \frac{\partial U}{\partial \rho} \right)_{T, \mu\nu_e} - \frac{U+P}{\rho} - \mu\nu_e n \left( \frac{\partial Y_L}{\partial \rho} \right)_{T, \mu\nu_e} \right] + \frac{\mathbf{k} \cdot [\mathbf{F} - \mu\nu_e \mathbf{F}_L]}{\rho} \right\} \delta\rho \\ + i \left( \frac{\partial P}{\partial \mu\nu_e} \right)_{\rho, T} \frac{\pi^2 \kappa_0 \rho}{k^2 \mathcal{K}} \times \left\{ n \omega \left( \frac{\partial Y_L}{\partial \rho} \right)_{T, \mu\nu_e} + \frac{\mathbf{k} \cdot \mathbf{F}_L}{\rho} \right\} \delta\rho. \end{aligned} \quad (56)$$

<sup>8</sup> By ‘‘isomeric’’ we mean that the composition of a fluid element is fixed. However, this is somewhat misleading. Only when the chemical potentials of all of the individual particle species are fixed can the composition be thought of as being frozen in. In the limit of rapid electron-type neutrino diffusion, the chemical potential of the neutrino is fixed over a wavelength to lowest  $\mathcal{O}(k^{-1})$ . Therefore, the relative concentrations of electrons, protons, and neutrons may evolve subject to the constraint  $\delta\mu_p + \delta\mu_e - \delta\mu_n = \delta\mu\nu_e = 0$ .

#### 4.1. A Note on The First Law of Thermodynamics in the Limit of Rapid Neutrino Diffusion

Here, we resort to the first law of thermodynamics

$$dE = TdS - PdV + \sum_i \mu_i dN_i \quad (57)$$

in order to gain insight into the results accumulated thus far. It is convenient to write the first law in terms of  $U = E/V$  and  $Y_L$  rather than  $E$  and  $N_i$  i.e.,

$$dU - \frac{U+P}{\rho}d\rho = nT ds + n\mu_{\nu_e} dY_L, \quad (58)$$

where  $s$  is the entropy per baryon. By differentiating with respect to density

$$nT \left( \frac{\partial s}{\partial \rho} \right)_{T, \mu_{\nu_e}} = \left( \frac{\partial U}{\partial \rho} \right)_{T, \mu_{\nu_e}} - \frac{U+P}{\rho} - \mu_{\nu_e} n \left( \frac{\partial Y_L}{\partial \rho} \right)_{T, \mu_{\nu_e}}, \quad (59)$$

we see that the right hand side yields the thermodynamic motivation for Silk damping, when compared to the appropriate terms in eqs. (52) and (56). If pressure leads density in time such that  $\delta P \propto -i\delta\rho$ , the mode will be damped. Thus, the criteria for Silk damping in PNSs is given by

$$nT \left( \frac{\partial s}{\partial \rho} \right)_{T, \mu_{\nu_e}} = \left( \frac{\partial U}{\partial \rho} \right)_{T, \mu_{\nu_e}} - \frac{U+P}{\rho} - \mu_{\nu_e} n \left( \frac{\partial Y_L}{\partial \rho} \right)_{T, \mu_{\nu_e}} < 0. \quad (60)$$

If the entropy of the fluid decreases upon an increase in density, then the fluid cools when compressed and is damped out (for now we are only considering the homogeneous case where the effects of the background  $\mathbf{F}$  and  $\mathbf{F}_L$  are small). Note however, that

$$\left( \frac{\partial U}{\partial \rho} \right)_{T, \mu_{\nu_e}} - \frac{U+P}{\rho} < 0 \quad \text{and} \quad \left( \frac{\partial Y_L}{\partial \rho} \right)_{T, \mu_{\nu_e}} < 0. \quad (61)$$

Hence, upon compression it is *possible* for radiative diffusion to heat the fluid rather than to cool it, making it possible for *radiative diffusion to drive compressible perturbations unstable*. In the  $\mu_{\nu_e} \rightarrow 0$  limit, cooling necessarily accompanies compression as in the case of classical Silk damping, where neutrinos only carry heat along with them as they diffuse down a temperature gradient. To show this, we again exploit the first law

$$\frac{dU}{dt} - \frac{U+P}{\rho} \frac{d\rho}{dt} = -\nabla \cdot \mathbf{F} = nT \frac{ds}{dt} + n\mu_{\nu_e} \frac{dY_L}{dt} \quad (62)$$

where  $\mathbf{F}$  denotes the flux of *energy*. When the chemical potential of the radiation is zero, the energy flux mediates the transport of heat alone. To further illustrate this point, we re-write the first law as

$$nT \frac{ds}{dt} = -\nabla \cdot [\mathbf{F} - \mu_{\nu_e} \mathbf{F}_L] - \mathbf{F}_L \cdot \nabla \mu_{\nu_e} \quad (63)$$

Burrows, Mazurek, and Lattimer (1981) noted that the second term on the right hand side is always positive for global cooling models of PNSs and therefore, always leads to heating as neutrinos escape. Those authors refer to this effect as ‘‘Joule heating’’ in analogy with the well known effect in electrodynamics.<sup>9</sup> Upon perturbation, the first law becomes

$$-i\omega nT [\delta s + \boldsymbol{\xi} \cdot \nabla s] = -i\mathbf{k} \cdot [\delta \mathbf{F} - \mu_{\nu_e} \delta \mathbf{F}_L] + \delta \mu_{\nu_e} \nabla \cdot \mathbf{F}_L, \quad (64)$$

where last term on the right hand side vanishes since  $\mathbf{F}_L$  is a constant for our equilibrium. This leaves us with

$$-i\omega nT \delta s \simeq -i\mathbf{k} \cdot [\delta \mathbf{F} - \mu_{\nu_e} \delta \mathbf{F}_L] = -i\mathbf{k} \cdot \delta \mathbf{F}_Q \quad (65)$$

where  $\delta \mathbf{F}_Q$  can be thought of as a heat flux and is responsible for cooling the perturbations via radiative diffusion. From eqs. (17)-(20), the heat flux  $\mathbf{F}_Q \equiv \mathbf{F} - \mu_{\nu_e} \mathbf{F}_L$  only depends on gradients in temperature i.e., heat is transported via changes in temperature alone. Burrows & Lattimer (1986) point out that this is due to our parameterization of opacity, which depends on the square of energy rather than on energy and composition. Thus, the temperature perturbation in the limit of rapid neutrino diffusion given by eq. (52) can be written in a more compact, yet descriptive form

$$\delta T \simeq i \frac{\kappa_{\text{eff}} \rho}{k^2 \mathcal{K} k_B^2 T} \times \left[ \omega nT \left( \frac{\partial s}{\partial \rho} \right)_{T, \mu_{\nu_e}} + \frac{\mathbf{k} \cdot \mathbf{F}_Q}{\rho} \right] \delta \rho. \quad (66)$$

Compare eq. (46) with eq. (66). Clearly, the entropy content of a fluid element is tied to its temperature perturbation while its lepton fraction is tied to fluctuations in the neutrino chemical potential. This reinforces the concept that heat flows down gradients in temperature while degeneracy energy is transported due to gradients in neutrino chemical potential.

<sup>9</sup> This point is made clear by realizing that  $\mathbf{F}_L \cdot \nabla \mu_{\nu_e} = -|\mathbf{F}_L|^2 / \sigma$  where  $\sigma$  is the radiative conductivity associated with lepton diffusion and that the lepton flux  $\mathbf{F}_L$  can be thought of as a current density.

#### 4.2. The Possibility of Diffusive Heating of Compressible Waves

In the limit of rapid neutrino diffusion, if the entropy of a compressed fluid element increases appreciably to counter the loss of degeneracy pressure that accompanies lepton transport, then the fluctuation gains energy during an oscillation. The criterion for this to occur and its applicability to PNSs is sketched out in Appendix B.

The entropy of a fluid element increases if the baryons exhibit some level of degeneracy as in the case of PNS cores. In order to illustrate this property, compare the ‘‘Silk determinant’’ for an ideal non-relativistic, non-degenerate gas of baryons ( $P \propto \rho T$ ) with that of a completely degenerate non-interacting and non-relativistic gas of baryons

$$\frac{\partial s_{\text{ideal}}}{\partial \rho} = \frac{\partial U}{\partial \rho} - \frac{U+P}{\rho} = -\frac{P}{\rho} < 0 \quad \text{while} \quad \frac{\partial s_{\text{deg}}}{\partial \rho} = 0. \quad (67)$$

The fact that the entropy response of a degenerate gas vanishes follows directly from the third law of thermodynamics. In other words, a purely degenerate gas is adiabatic by *fiat* since it contains zero entropy. Furthermore, in a mixture of baryons consisting of protons and neutrons in the core of PNSs, the total equation of state may be super-adiabatic in the sense that the net entropy increases upon compression. Consider the zero-point energy density of the neutrons given by eq. (B3). The estimate given in Appendix B indicates that upon compression, the entropy of the neutrons increases in the limit of rapid neutrino diffusion. An increase in density necessarily leads to a decrease in lepton fraction  $Y_L$  due to overall charge neutrality. The removal of a proton, which results from deleptonization, and the addition of a neutron results in a net increase in pressure or energy per unit volume upon compression since the chemical potential i.e., Fermi energy, of the neutrons is greater than that of the protons.

Another positive contribution to the Silk determinant originates from changes in electron pressure or energy density resulting from changes in density. Though the electron pressure does not explicitly depend on fluid density, it implicitly does through the electron chemical potential and the condition for chemical equilibrium. In the limit of large electron degeneracy, the electron pressure  $U_e = 3P_e \propto \mu_e^4$ . Therefore, changes in  $U_e$  result from changes in  $\mu_e$ . The condition for chemical equilibrium, eq. (30), informs us that  $\mu_e$  increases by a factor of  $k_B T (Y_p/Y_n)$  upon compression. Eq. (B6) displays this point.

The deleptonization of a fluid element contributes to the Silk determinant, quantified by the term  $\propto \mu_{\nu_e} \partial Y_L / \partial \rho$  at fixed temperature  $T$  and neutrino chemical potential  $\mu_{\nu_e}$ . It is tempting to equate the phenomenon of heating due to deleptonization for compressible waves to Joule heating. Such a comparison would be misleading at best. Rather than an energy deposition mechanism  $\propto |\mathbf{F}_L|^2$ , this is a purely linear phenomenon. The Silk determinant, which is  $\propto (\partial s / \partial \rho)$  at constant  $T$  and  $\nu_e$ , denotes only the entropy evolution of a fluid element. The deleptonization term merely acts to enforce that the heat content of the neutrinos, rather than heat and degeneracy energy, is being taken into account as the entropy of a fluid element changes during compression.

The sum of all these actions together must overcome the loss of degeneracy pressure accompanied by deleptonization. Damping due to loss of lepton pressure is provided by the component of the pressure perturbation that originates from changes in chemical potential. This effect occurs in global cooling models of PNSs as well (Burrows, Mazurek, & Lattimer 1981). Not only is thermal energy altered by neutrino diffusion, but the large lepton degeneracy energy (particularly in the core) is lost as well. Loss of lepton pressure resulting from neutrino diffusion always damps out compressible motion.

### 5. COUPLING OF MAGNETOSONIC MOTION TO THE BACKGROUND NEUTRINO FLUX: NEUTRINO BUBBLES

Below we derive the stability criteria and growth rates for the fast and slow neutrino bubble instability while explaining the nature of the driving mechanism as well. Two distinct, yet equivalent, interpretations of these radiative magnetoacoustic instabilities will be presented. One comes from understanding the relationship between the radiation pressure and density perturbations. If radiation pressure lags behind density (in time), heating accompanies compression – the necessary criterion for driving. In the frame of the fluid element, the radiation pressure perturbation is composed of three distinct components. The balance between the three components ultimately determines the stability properties of the magnetoacoustic mode. Another way of understanding radiative magnetoacoustic driving is by examining the relationship between the fluid velocity (or displacement) and the perturbed radiation force. The radiation force perpendicular to the wave vector is given by the sum of the perpendicular components of the linear energy and lepton flux perturbation. This drives magnetosonic motion unstable since the fluid oscillates in part along the magnetic field line. That is, the uniform background magnetic field  $\mathbf{B}$  may in general, lie in any direction with respect to the wave vector  $\mathbf{k}$ , allowing the motion of the fluid and the radiative driving force to coincide, leading to a net over-stability.

We first identify the basic properties of standard magnetosonic waves in the absence of stratification and radiative diffusion. In order to understand neutrino bubble instability from the relationship between pressure and density perturbations, we calculate the growth rates by use of the magnetosonic wave equation and isolate the relevant components of the pressure perturbation that lead to damping and driving. We then perform the exact same analysis on the linearized equation of motion where the component of the perturbed radiative energy and lepton flux perpendicular to the wave vector drives magnetosonic modes unstable.

#### 5.1. Basic Magnetosonic Waves

Linearizing the continuity, momentum, and induction equations, as well as Gauss’ Law, yields

$$-i\omega\delta\rho + i\rho\mathbf{k} \cdot \delta\mathbf{v} + \delta\mathbf{v} \cdot \nabla\rho = 0, \quad (68)$$

$$-i\omega\rho\delta\mathbf{v} = -i\mathbf{k}\delta P + \mathbf{g}\delta\rho + \frac{i}{4\pi}(\mathbf{k} \times \delta\mathbf{B}) \times \mathbf{B}, \quad (69)$$

$$-i\omega\delta\mathbf{B} = i\mathbf{k} \times (\delta\mathbf{v} \times \mathbf{B}), \quad (70)$$

and

$$\mathbf{k} \cdot \delta\mathbf{B} = 0, \quad (71)$$

respectively.

The procedure for obtaining the asymptotic growth rate for radiatively driven magnetoacoustic instabilities was carried out in detail by BS03. Based on analysis of the general (and cumbersome) dispersion relation, they concluded that in the short wave-length limit, the radiatively driven MHD instabilities behaved as the standard fast and slow magnetoacoustic modes to lowest order where the effects of radiation produced a relatively small imaginary correction to the mode frequency. In order to isolate the mechanism for over-stability, BS03 then performed an asymptotic modal analysis where they solved the momentum equation by using the standard fast and slow eigenvectors and applied them to all of the  $\mathcal{O}(k^{-1})$  terms in the momentum equation; the pressure driving terms  $\propto \delta T$ , buoyancy force  $\propto \mathbf{g} \delta \rho$ , and to the Eulerian component of the the density perturbation which is  $\propto \delta \mathbf{v} \cdot \nabla \ln \rho$ . This technique is mathematically similar to the work integral approach in classic stellar pulsation theory (Unno 1989) for obtaining growth rates due to non-adiabatic driving of nearly adiabatic pulsations.

To lowest order, the linear momentum equation is given by

$$-i\omega\rho\delta\mathbf{v} = -i\mathbf{k} \left[ \delta P_{\text{ac}} + \frac{\mathbf{B} \cdot \delta\mathbf{B}}{4\pi} \right] + i \frac{\mathbf{k} \cdot \mathbf{B}}{4\pi} \delta\mathbf{B} \quad (72)$$

where  $\delta P_{\text{ac}} \equiv c_i^2 \delta \rho$  is the short-wavelength acoustic pressure response to a density perturbation  $\delta \rho$ . Also to lowest order,

$$\delta \rho = \rho \frac{\mathbf{k} \cdot \delta \mathbf{v}}{\omega} \quad \text{and} \quad \delta \mathbf{B} = \frac{\mathbf{B}}{\omega} (\mathbf{k} \cdot \delta \mathbf{v}) - \frac{\mathbf{k} \cdot \mathbf{B}}{\omega} \delta \mathbf{v}. \quad (73)$$

Eliminating  $\delta \mathbf{B}$ , we obtain

$$-i\rho \frac{\tilde{\omega}^2}{\omega} \delta \mathbf{v} = -i\mathbf{k} \left[ (c_i^2 + v_A^2) \delta \rho - c_i^2 \frac{(\mathbf{k} \cdot \mathbf{v}_A)^2}{\omega^2} \delta \rho \right] + i(\mathbf{k} \cdot \mathbf{v}_A) \mathbf{v}_A \delta \rho. \quad (74)$$

where  $\mathbf{v}_A = \mathbf{B}/\sqrt{4\pi\rho}$  is the Alfvén velocity and  $\tilde{\omega}^2 \equiv \omega^2 - (\mathbf{k} \cdot \mathbf{v}_A)^2$ . In the optically thick limit, neutrinos force the gas via a gradient in their pressure which is  $\parallel$  to  $\mathbf{k}$  in the short wave-length limit. This requires the waves to possess some longitudinal, or compressible, component which automatically rules out the purely incompressible shear Alfvén wave as a candidate for over-stable radiative driving. In order to isolate the magnetosonic fast and slow waves, let's define a mode polarization  $\hat{\mathbf{e}}(\omega, k)$  such that  $\delta \mathbf{v} = \hat{\mathbf{e}}(\omega, k) \psi(\omega, k)$  where  $\psi$  is some complex-valued amplitude. Choosing  $\psi = \delta \rho / \rho$  gives us the magnetosonic eigenvectors,

$$\hat{\mathbf{e}}(\omega, k) = \frac{\omega}{\tilde{\omega}^2} \left[ \left( \frac{\tilde{\omega}^2}{\omega^2} c_i^2 + v_A^2 \right) \mathbf{k} - (\mathbf{k} \cdot \mathbf{v}_A) \mathbf{v}_A \right] \quad (75)$$

where the two magnetosonic modes must satisfy the dispersion relation

$$\omega^2 = k^2 c_i^2 \frac{\tilde{\omega}^2}{\omega^2} + k^2 v_A^2. \quad (76)$$

In principle, the fast and slow modes posses components both  $\parallel$  and  $\perp$  to  $\mathbf{k}$ . This mixed longitudinal and transverse behavior is central to the MHD radiative driving mechanism (BS03), a point we will now discuss.

### 5.2. The Magnetosonic Wave Equation Subject to Rapid Radiative Diffusion: Asymptotic Growth Rate

Taking the divergence of eq. (69), immediately allows us to restrict our analysis to compressible short-wavelength motions i.e., the modes that can be driven unstable by the effects of radiative diffusion. We have

$$-i\omega \mathbf{k} \cdot \delta \mathbf{v} = -ik^2 \left[ \frac{\delta P}{\rho} + \frac{\mathbf{B} \cdot \delta \mathbf{B}}{4\pi\rho} \right] + (\mathbf{k} \cdot \mathbf{g}) \frac{\delta \rho}{\rho} \quad (77)$$

where we have made use of eq. (71). Eliminating  $\delta \mathbf{B}$  using eq. (70) gives us

$$-i\omega (\mathbf{k} \cdot \delta \mathbf{v}) = -ik^2 \left[ \frac{\delta P}{\rho} + v_A^2 \frac{(\mathbf{k} \cdot \delta \mathbf{v})}{\omega} - \frac{(\mathbf{k} \cdot \mathbf{v}_A)^2}{\omega^2} \frac{\delta P}{\rho} - i \frac{(\mathbf{g} \cdot \mathbf{v}_A)(\mathbf{k} \cdot \mathbf{v}_A)}{\omega^2} \frac{\delta \rho}{\rho} \right] + (\mathbf{k} \cdot \mathbf{g}) \frac{\delta \rho}{\rho}. \quad (78)$$

Dividing the pressure perturbation into its acoustic  $\delta P_{\text{ac}}$  and driving/damping  $\tilde{\delta P}$  contributions and by utilizing eq. (68), the magnetosonic wave equation becomes

$$\left[ \omega^2 - k^2 \frac{\tilde{\omega}^2}{\omega^2} c_i^2 - k^2 v_A^2 \right] \frac{\delta \rho}{\rho} \simeq -i\omega \delta \mathbf{v} \cdot \nabla \ln \rho + k^2 \left\{ \frac{\tilde{\omega}^2}{\omega^2} \frac{\tilde{\delta P}}{\rho} + iv_A^2 \frac{\delta \mathbf{v}}{\omega} \cdot \nabla \ln \rho - i \frac{(\mathbf{g} \cdot \mathbf{v}_A)(\mathbf{k} \cdot \mathbf{v}_A)}{\omega^2} \frac{\delta \rho}{\rho} \right\} + i(\mathbf{k} \cdot \mathbf{g}) \frac{\delta \rho}{\rho}. \quad (79)$$

Neglecting terms depending on background gradients or those originating from radiative diffusion leaves us with only the left hand side of eq. (79) i.e., the magnetosonic wave equation for a uniform background. The terms on the right hand side of eq. (79) produce  $\mathcal{O}(k^{-1})$  corrections to a magnetosonic wave and are responsible for the growth and damping rates which can be viewed as  $\mathcal{O}(k^{-1})$  corrections to the mode frequency. In order to evaluate the frequency correction arising from radiative driving, we let  $\omega \rightarrow \omega + A_0$ , where  $A_0$  is the damping or driving rate which is independent of the wavenumber  $k$ .

It is useful to recast the gravitational acceleration,  $\mathbf{g}$ , by using hydrostatic balance

$$\mathbf{g} = \frac{1}{\rho} \nabla P = c_i^2 \nabla \ln \rho + \frac{1}{\rho} \left[ \left( \frac{\partial P}{\partial T} \right)_{\rho, \mu_{\nu_e}} \nabla T + \left( \frac{\partial P}{\partial \mu_{\nu_e}} \right)_{\rho, T} \nabla \mu_{\nu_e} \right]. \quad (80)$$

This, along with the magnetosonic polarization vector given by eq. (75) allows us to eliminate all of the terms  $\propto \nabla \ln \rho$  in eq. (79). The asymptotic prescription for the eigenvalues mentioned above allows us to convert eq. (79) into an expression for the damping or driving rate. After a bit of algebra, we have

$$\begin{aligned} \frac{2A_0}{\omega} [2\omega^2 - k^2 (c_i^2 + v_A^2)] \frac{\delta\rho}{\rho} \simeq k^2 \left\{ \frac{\tilde{\omega}^2 \delta\tilde{P}}{\omega^2 \rho} - i \frac{(\mathbf{k} \cdot \mathbf{v}_A)}{\omega^2 \rho} \mathbf{v}_A \cdot \left[ \left( \frac{\partial P}{\partial T} \right)_{\rho, \mu_{\nu_e}} \nabla T + \left( \frac{\partial P}{\partial \mu_{\nu_e}} \right)_{\rho, T} \nabla \mu_{\nu_e} \right] \frac{\delta\rho}{\rho} \right\} \\ + i \frac{\mathbf{k}}{\rho} \cdot \left[ \left( \frac{\partial P}{\partial T} \right)_{\rho, \mu_{\nu_e}} \nabla T + \left( \frac{\partial P}{\partial \mu_{\nu_e}} \right)_{\rho, T} \nabla \mu_{\nu_e} \right] \frac{\delta\rho}{\rho}. \end{aligned} \quad (81)$$

If we expand  $\delta\tilde{P}$  by use of eq. (56) while noting that

$$\nabla T = -\frac{\kappa_{\text{eff}} \rho}{\mathcal{K} k_B^2 T} [\mathbf{F} - \mu_{\nu_e} \mathbf{F}_L] \quad \text{and} \quad \nabla \mu_{\nu_e} = -\frac{\pi^2 \kappa_0 \rho}{\mathcal{K}} \mathbf{F}_L, \quad (82)$$

the growth rate  $A_0$  from eq. (81) is given by

$$\begin{aligned} A_0 = \frac{i}{2 [2\omega^2 - k^2 (c_i^2 + v_A^2)]} \times \left\{ \frac{\pi^2 \kappa_0}{\mathcal{K}} \left( \frac{\partial P}{\partial \mu_{\nu_e}} \right)_{\rho, T} \left[ \rho \tilde{\omega}^2 n \left( \frac{\partial Y_L}{\partial \rho} \right)_{\rho, \mu_{\nu_e}} + \frac{(\mathbf{k} \cdot \mathbf{v}_A)}{\omega} (\mathbf{k} \times \mathbf{v}_A) \cdot (\mathbf{k} \times \mathbf{F}_L) \right] \right. \\ \left. + \frac{\kappa_{\text{eff}}}{\mathcal{K} k_B^2 T} \left( \frac{\partial P}{\partial T} \right)_{\rho, \mu_{\nu_e}} \left[ \rho \tilde{\omega}^2 \left( \left( \frac{\partial U}{\partial \rho} \right)_{T, \mu_{\nu_e}} - \frac{U+P}{\rho} - \mu_{\nu_e} n \left( \frac{\partial Y_L}{\partial \rho} \right)_{T, \mu_{\nu_e}} \right) + \frac{(\mathbf{k} \cdot \mathbf{v}_A)}{\omega} (\mathbf{k} \times \mathbf{v}_A) \cdot (\mathbf{k} \times [\mathbf{F} - \mu_{\nu_e} \mathbf{F}_L]) \right] \right\}. \end{aligned} \quad (83)$$

### 5.3. Analogy with the Work Integral

BS03 noticed that when the components of the radiation pressure perturbation originating from gradients in background quantities are non-zero, radiative driving may then occur. Consider the Lagrangian perturbation of the total neutrino pressure defined as

$$\Delta P_\nu \equiv \Delta [P_{\nu_e} + P_{\bar{\nu}_e} + P_{\nu_x} + P_{\bar{\nu}_x}] = \boldsymbol{\xi} \cdot \nabla P_\nu + \delta P_\nu \quad (84)$$

where  $\boldsymbol{\xi} = i\delta\mathbf{v}/\omega$  is the fluid's Lagrangian displacement. More explicitly,

$$\Delta P_\nu = \left( \frac{\partial P_\nu}{\partial T} \right)_{\mu_{\nu_e}} \boldsymbol{\xi} \cdot \nabla T + \left( \frac{\partial P_\nu}{\partial \mu_{\nu_e}} \right)_T \boldsymbol{\xi} \cdot \nabla \mu_{\nu_e} + \left( \frac{\partial P_\nu}{\partial T} \right)_{\mu_{\nu_e}} \delta T + \left( \frac{\partial P_\nu}{\partial \mu_{\nu_e}} \right)_T \delta \mu_{\nu_e}. \quad (85)$$

The density dependence in the pressure derivatives is discarded since  $P_\nu$  depends only on temperature and neutrino chemical potential. By using eqs. (46), (52), and (82), the driving component of  $\Delta P_\nu$  becomes

$$\begin{aligned} \Delta P_\nu^{\text{drive}} = - \left( \frac{\partial P_\nu}{\partial T} \right)_{\mu_{\nu_e}} \frac{\kappa_{\text{eff}} \rho}{\mathcal{K} k_B^2 T k^2} \left\{ k^2 \boldsymbol{\xi} \cdot [\mathbf{F} - \mu_{\nu_e} \mathbf{F}_L] - \mathbf{k} \cdot [\mathbf{F} - \mu_{\nu_e} \mathbf{F}_L] (\mathbf{k} \cdot \boldsymbol{\xi}) \right\} - \left( \frac{\partial P_\nu}{\partial \mu_{\nu_e}} \right)_T \frac{\pi^2 \kappa_0 \rho}{\mathcal{K} k^2} \left\{ k^2 \boldsymbol{\xi} \cdot \mathbf{F}_L - \mathbf{k} \cdot \mathbf{F}_L (\mathbf{k} \cdot \boldsymbol{\xi}) \right\} \\ = - \left( \frac{\partial P_\nu}{\partial T} \right)_{\mu_{\nu_e}} \frac{\kappa_{\text{eff}} \rho}{\mathcal{K} k_B^2 T k^2} \left\{ (\mathbf{k} \times \boldsymbol{\xi}) \cdot (\mathbf{k} \times [\mathbf{F} - \mu_{\nu_e} \mathbf{F}_L]) \right\} - \left( \frac{\partial P_\nu}{\partial \mu_{\nu_e}} \right)_T \frac{\pi^2 \kappa_0 \rho}{\mathcal{K} k^2} \left\{ (\mathbf{k} \times \boldsymbol{\xi}) \cdot (\mathbf{k} \times \mathbf{F}_L) \right\}, \end{aligned} \quad (86)$$

and by using the magnetosonic eigenvector given by eq. (75), the driving component becomes

$$\begin{aligned} \Delta P_\nu^{\text{drive}} = i \frac{(\mathbf{k} \cdot \mathbf{v}_A)}{\tilde{\omega}^2} \left( \frac{\partial P_\nu}{\partial T} \right)_{\mu_{\nu_e}} \frac{\kappa_{\text{eff}} \rho}{\mathcal{K} k_B^2 T k^2} \left\{ (\mathbf{k} \times \mathbf{v}_A) \cdot (\mathbf{k} \times [\mathbf{F} - \mu_{\nu_e} \mathbf{F}_L]) \right\} \frac{\delta\rho}{\rho} \\ + i \frac{(\mathbf{k} \cdot \mathbf{v}_A)}{\tilde{\omega}^2} \left( \frac{\partial P_\nu}{\partial \mu_{\nu_e}} \right)_T \frac{\pi^2 \kappa_0 \rho}{\mathcal{K} k^2} \left\{ (\mathbf{k} \times \mathbf{v}_A) \cdot (\mathbf{k} \times \mathbf{F}_L) \right\} \frac{\delta\rho}{\rho}. \end{aligned} \quad (87)$$

If the radiation pressure maximum is attained after the fluid's density maximum, there will be a net amount of work during the compression cycle. Thus, the criterion for instability via radiative driving can be written as

$$\text{Im} [\Delta\rho^* \Delta P_\nu] > 0 \quad (88)$$

where  $\Delta\rho = \delta\rho + \boldsymbol{\xi} \cdot \nabla\rho$  is the Lagrangian density perturbation. It can be checked that upon substitution of eq. (87) into the above expression, the same criteria over-stability is obtained as that given by eq. (83).

To gain a deeper understanding of the driving mechanism, consider purely hydrodynamic acoustic motion where  $\mathbf{B} = \mathbf{v}_A = 0$  such that  $\boldsymbol{\xi} \parallel \mathbf{k}$ . Substituting an appropriate sound wave eigenvector into eq. (86), we see that

$$\Delta P_\nu^{\text{drive}} \propto \left( \frac{\partial P_\nu}{\partial T} \right)_{\mu_{\nu_e}} \frac{\kappa_{\text{eff}} \rho}{\mathcal{K} k_B^2 T k^2} \left\{ k^2 \mathbf{k} \cdot [\mathbf{F} - \mu_{\nu_e} \mathbf{F}_L] - \mathbf{k} \cdot [\mathbf{F} - \mu_{\nu_e} \mathbf{F}_L] (\mathbf{k} \cdot \mathbf{k}) \right\} + \left( \frac{\partial P_\nu}{\partial \mu_{\nu_e}} \right)_T \frac{\pi^2 \kappa_0 \rho}{\mathcal{K} k^2} \left\{ k^2 \mathbf{k} \cdot \mathbf{F}_L - \mathbf{k} \cdot \mathbf{F}_L (\mathbf{k} \cdot \mathbf{k}) \right\} = 0. \quad (89)$$

That is, for purely hydrodynamic sound waves, radiative driving vanishes due to an exact cancellation of two unique effects, which we describe below.

Regardless of the direction in which a fluid oscillates, the background radiative fluxes  $\mathbf{F}$  and  $\mathbf{F}_L$  always force a fluid element if there is a change in density. We call this effect ‘‘shadowing,’’ following the terminology of the O star line-driven wind literature (Lucy & White 1980, Lucy 1982). For the sake of exposition, let's ignore lepton number and assume that  $\mathbf{F}_L = \mu_{\nu_e} = 0$ . The component



of the Lagrangian pressure perturbation due to shadowing originates from the  $\nabla \cdot \delta \mathbf{F}$  term in the first law of thermodynamics and is present in eq. (56) i.e.,

$$\Delta P_\nu^{\text{shadow}} = i \left( \frac{\partial P_\nu}{\partial T} \right) \frac{\kappa_{\text{eff}}}{k^2 \mathcal{K} k_B^2 T} (\mathbf{k} \cdot \mathbf{F}) \delta \rho = -i \left( \frac{\partial P_\nu}{\partial T} \right) \frac{\mathbf{k} \cdot \nabla T}{k^2} \frac{\delta \rho}{\rho} = - \left( \frac{\partial P_\nu}{\partial T} \right) \frac{\mathbf{k} \cdot \nabla T}{k^2} (\mathbf{k} \cdot \boldsymbol{\xi}). \quad (90)$$

Radiation piles up before the density maximum as the local decrease in mean free path temporarily hinders the transmission of quanta (Baker & Kippenhahn 1962). However, the total extinction over a wavelength remains the same since a fluid element's mass is a constant during the compression cycle. In order to conserve quanta, a deficit of radiation, or a shadow, appears upstream of the density maximum. The surplus of radiation downstream and the deficit of radiation upstream of the density maximum induces a pressure differential that peaks at the point of maximum density along the wave.

The contribution to the Lagrangian radiation pressure perturbation due to changes in the displacement vector  $\boldsymbol{\xi}$  is given by

$$\Delta P_\nu^{\text{displace}} = \boldsymbol{\xi} \cdot \nabla P_\nu = \left( \frac{\partial P_\nu}{\partial T} \right) \boldsymbol{\xi} \cdot \nabla T. \quad (91)$$

When a fluid element moves upward along the direction of  $\mathbf{F}$ , the background pressure it samples is smaller than the value at its original position. Conversely, when a fluid element moves downward, the radiation pressure perturbation increases. As previously mentioned, if  $\boldsymbol{\xi} \parallel \mathbf{k}$  as in the case of a purely hydrodynamic sound waves, the pressure perturbations from shadowing and motion along the temperature gradient cancel one another out, a point clearly seen when comparing eqs. (90) and (91).

This harmony between  $\Delta P_\nu^{\text{shadow}}$  and  $\Delta P_\nu^{\text{displace}}$  is broken when the magnetic field is introduced. The change in radiation pressure due to a change in position does not in general match the acoustic response followed by a change in density since the fluid element oscillates in part along the direction of the equilibrium  $\mathbf{B}$ .

#### 5.4. Limit of Blaes & Socrates 2003

The instability mechanism considered in BS03 is essentially the same as in this work. The major difference was their assumption of zero chemical potential for the photon radiation field as they were considering backgrounds that were close to perfect black bodies. Setting  $\mu_{\nu_e} = (\partial P / \partial \mu_{\nu_e}) = 0$  in eq. (83) we have

$$A_0 = \frac{i}{2 [2\omega^2 - k^2 (c_i^2 + v_A^2)]} \times \left\{ \frac{\kappa_{\text{eff}}}{\mathcal{K} k_B^2 T} \left( \frac{\partial P}{\partial T} \right)_{\rho, \mu_{\nu_e}} \left[ \rho \tilde{\omega}^2 \left( \left( \frac{\partial U}{\partial \rho} \right)_{T, \mu_{\nu_e}} - \frac{U+P}{\rho} \right) + \frac{(\mathbf{k} \cdot \mathbf{v}_A)}{\omega} (\mathbf{k} \times \mathbf{v}_A) \cdot (\mathbf{k} \times \mathbf{F}) \right] \right\}, \quad (92)$$

which is completely equivalent to the one-temperature MHD growth rates given by eqs. (93) and (107) of BS03.

#### 5.5. Magnetosonic Waves Forced by Radiative Diffusion: The Perpendicular Radiation Force

An alternative, and more visual, physical picture for these instabilities arises from considering forces on oscillating fluid elements. For this particular application, it is both helpful and revealing to adopt the Lagrangian displacement  $\boldsymbol{\xi}$  as our fundamental fluid variable. Other important fluid quantities are related to  $\boldsymbol{\xi}$  in the following way

$$\delta \mathbf{B} = \nabla \times (\boldsymbol{\xi} \times \mathbf{B}) = i \mathbf{k} \times (\boldsymbol{\xi} \times \mathbf{B}), \quad \frac{\delta \rho}{\rho} = -i (\mathbf{k} \cdot \boldsymbol{\xi}) - \boldsymbol{\xi} \cdot \nabla \ln \rho, \quad \text{and} \quad \frac{\delta P_{\text{ac}}}{\rho} = -i c_i^2 (\mathbf{k} \cdot \boldsymbol{\xi}) - c_i^2 \boldsymbol{\xi} \cdot \nabla \ln \rho. \quad (93)$$

This allows us to write the Euler equation, eq. (69) in terms of Lagrangian displacements

$$\frac{\partial^2 \boldsymbol{\xi}}{\partial t^2} \simeq -(\mathbf{k} \cdot \mathbf{v}_A)^2 \boldsymbol{\xi} - \mathbf{k} (c_i^2 + v_A^2) (\mathbf{k} \cdot \boldsymbol{\xi}) + \mathbf{v}_A (\mathbf{k} \cdot \mathbf{v}_A) (\mathbf{k} \cdot \boldsymbol{\xi}) + \mathbf{k} (\mathbf{k} \cdot \mathbf{v}_A) (\boldsymbol{\xi} \cdot \mathbf{v}_A) - i \mathbf{k} \left[ \frac{\delta \tilde{P}_{\text{damp}}}{\rho} + \frac{\delta \tilde{P}_{\text{drive}}}{\rho} - c_i^2 \boldsymbol{\xi} \cdot \nabla \ln \rho \right] - i \mathbf{g} (\mathbf{k} \cdot \boldsymbol{\xi}) \quad (94)$$

where  $\delta \tilde{P} = \delta \tilde{P}_{\text{drive}} + \delta \tilde{P}_{\text{damp}}$  and from eq. (56)

$$\delta \tilde{P}_{\text{drive}} \equiv i \left( \frac{\partial P}{\partial T} \right)_{\rho, \mu_{\nu_e}} \frac{\kappa_{\text{eff}} \rho}{k^2 \mathcal{K} k_B^2 T} (\mathbf{k} \cdot [\mathbf{F} - \mu_{\nu_e} \mathbf{F}_L]) \frac{\delta \rho}{\rho} + i \left( \frac{\partial P}{\partial \mu_{\nu_e}} \right)_{\rho, T} \frac{\pi^2 \kappa_0 \rho}{k^2 \mathcal{K}} (\mathbf{k} \cdot \mathbf{F}_L) \frac{\delta \rho}{\rho}. \quad (95)$$

The lowest order acoustic and magnetic tension restoring force terms on the right hand side of eq. (94) can be reduced to

$$(\mathbf{k} \cdot \mathbf{v}_A)^2 \boldsymbol{\xi} + \mathbf{k} (c_i^2 + v_A^2) (\mathbf{k} \cdot \boldsymbol{\xi}) - \mathbf{v}_A (\mathbf{k} \cdot \mathbf{v}_A) (\mathbf{k} \cdot \boldsymbol{\xi}) - \mathbf{k} (\mathbf{k} \cdot \mathbf{v}_A) (\boldsymbol{\xi} \cdot \mathbf{v}_A) = k^2 v_{\text{ph}}^2 \boldsymbol{\xi} \quad (96)$$

by use of eqs. (75) and (76) where  $v_{\text{ph}}^2 \equiv \omega^2 / k^2$  is the square of the phase velocity. The local gravitational acceleration  $\mathbf{g}$  can be expressed in terms of the radiative and lepton fluxes by use of hydrostatic balance given by eq. (80) and eq. (82) such that

$$\mathbf{g} = c_i^2 \nabla \ln \rho - \left( \frac{\partial P}{\partial T} \right)_{\rho, \mu_{\nu_e}} \frac{\kappa_{\text{eff}}}{\mathcal{K} k_B^2 T} [\mathbf{F} - \mu_{\nu_e} \mathbf{F}_L] - \left( \frac{\partial P}{\partial \mu_{\nu_e}} \right)_{\rho, T} \frac{\pi^2 \kappa_0}{\mathcal{K}} \mathbf{F}_L. \quad (97)$$

Inserting this into the equation of motion yields

$$\begin{aligned} \frac{\partial^2 \boldsymbol{\xi}}{\partial t^2} + k^2 v_{\text{ph}}^2 \boldsymbol{\xi} \simeq & -i \mathbf{k} \frac{\delta \tilde{P}_{\text{damp}}}{\rho} - i \mathbf{k} \frac{(\mathbf{k} \cdot \boldsymbol{\xi})}{k^2} \mathbf{k} \cdot \left[ \left( \frac{\partial P}{\partial T} \right)_{\rho, \mu_{\nu_e}} \frac{\kappa_{\text{eff}}}{\mathcal{K} k_B^2 T} [\mathbf{F} - \mu_{\nu_e} \mathbf{F}_L] + \left( \frac{\partial P}{\partial \mu_{\nu_e}} \right)_{\rho, T} \frac{\pi^2 \kappa_0}{\mathcal{K}} \mathbf{F}_L \right] \\ & + i (\mathbf{k} \cdot \boldsymbol{\xi}) \left[ \left( \frac{\partial P}{\partial T} \right)_{\rho, \mu_{\nu_e}} \frac{\kappa_{\text{eff}}}{\mathcal{K} k_B^2 T} [\mathbf{F} - \mu_{\nu_e} \mathbf{F}_L] + \left( \frac{\partial P}{\partial \mu_{\nu_e}} \right)_{\rho, T} \frac{\pi^2 \kappa_0}{\mathcal{K}} \mathbf{F}_L \right] + i \mathbf{k} c_i^2 \boldsymbol{\xi} \cdot \nabla \ln \rho - i (\mathbf{k} \cdot \boldsymbol{\xi}) c_i^2 \nabla \ln \rho. \end{aligned} \quad (98)$$

The driving terms on the right hand side of eq. (98) may be recast in the following form

$$-i \left( \frac{\partial P}{\partial T} \right)_{\rho, \mu_{\nu_e}} \frac{\kappa_{\text{eff}}}{\mathcal{K} k_B^2 T} \left( \frac{\mathbf{k}\mathbf{k}}{k^2} - \mathbf{1} \right) \cdot [\mathbf{F} - \mu_{\nu_e} \mathbf{F}_L] (\mathbf{k} \cdot \boldsymbol{\xi}) - i \left( \frac{\partial P}{\partial \mu_{\nu_e}} \right)_{\rho, T} \frac{\pi^2 \kappa_0}{\mathcal{K}} \left( \frac{\mathbf{k}\mathbf{k}}{k^2} - \mathbf{1} \right) \cdot \mathbf{F}_L (\mathbf{k} \cdot \boldsymbol{\xi}) + i c_1^2 \boldsymbol{\xi} \times (\mathbf{k} \times \nabla \ln \rho) \quad (99)$$

where the last term is orthogonal to fluid displacements and therefore cannot drive the mode. Ultimately, the linear radiation force per unit mass  $\delta \mathcal{F}_{\text{rad}}$  is given by a gradient in the total neutrino pressure  $= -\frac{1}{\rho} \nabla [P_{\nu_e} + P_{\bar{\nu}_e} + P_{\nu_x}]$  and upon perturbation

$$\delta \mathcal{F}_{\text{rad}} = \frac{1}{\rho} \nabla P_{\nu} \frac{\delta \rho}{\rho} - i \frac{\mathbf{k}}{\rho} \delta P_{\nu}. \quad (100)$$

where  $P_{\nu} = P_{\nu_e} + P_{\bar{\nu}_e} + P_{\nu_x}$ . Following the discussion surrounding eq. (65), the first term may be broken into a component which carries heat and one that carries lepton number

$$\frac{1}{\rho} \nabla P_{\nu} \frac{\delta \rho}{\rho} = i \left( \frac{\partial P_{\nu}}{\partial T} \right)_{\rho, \mu_{\nu_e}} \frac{\kappa_{\text{eff}}}{\mathcal{K} k_B^2 T} \mathbf{F}_Q (\mathbf{k} \cdot \boldsymbol{\xi}) + i \left( \frac{\partial P_{\nu}}{\partial \mu_{\nu_e}} \right)_{\rho, T} \frac{\pi^2 \kappa_0}{\mathcal{K}} \mathbf{F}_L (\mathbf{k} \cdot \boldsymbol{\xi}) \quad (101)$$

where we have kept the leading terms  $\delta \rho$ , the linear driving force  $\delta \mathcal{F}_{\text{drive}}$  can be written in terms of the two perturbed fluxes

$$\delta \mathcal{F}_{\text{drive}} = \hat{\mathbf{k}} \times \delta \mathcal{F}_{\text{rad}} = \hat{\mathbf{k}} \times \left[ \left( \frac{\partial P_{\nu}}{\partial T} \right)_{\rho, \mu_{\nu_e}} \frac{\kappa_{\text{eff}}}{\mathcal{K} k_B^2 T} \delta \mathbf{F}_Q + \left( \frac{\partial P_{\nu}}{\partial \mu_{\nu_e}} \right)_{\rho, T} \frac{\pi^2 \kappa_0}{\mathcal{K}} \delta \mathbf{F}_L \right]. \quad (102)$$

Thus, the component of the perturbed heat and lepton flux  $\perp$  to  $\mathbf{k}$  leads to secular driving of the magnetoacoustic waves (see Figure 2). Due to magnetic tension, the fast and slow magnetoacoustic waves possess polarizations which have components along  $\mathbf{B}$ , which in general, are *not*  $\parallel$  to  $\mathbf{k}$ . Note that  $\delta \mathcal{F}_{\text{drive}}$  is the driving force originating from radiation pressure alone. As previously argued, changes

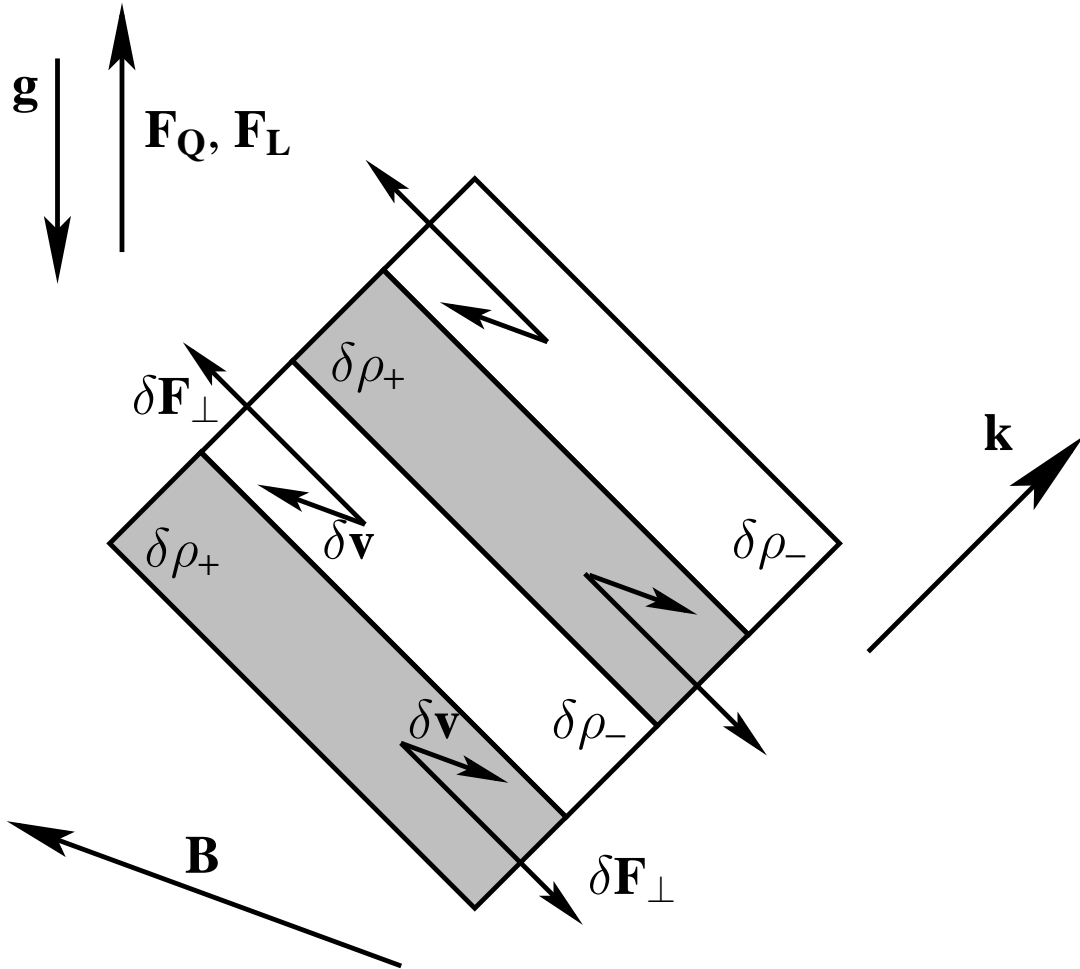


FIG. 2.— Geometry of the neutrino bubble instability. Here,  $\delta \mathbf{F}_\perp$  is any general perpendicular radiative flux, which denotes the direction of both  $\delta \mathbf{F}_L$  and  $\delta \mathbf{F}_Q$  – assuming that the equilibrium  $\mathbf{F}_Q$  and  $\mathbf{F}_L$  lie in the same direction. For the sake of clarity, the polarization properties of the depicted wave are that of the slow magnetosonic wave in the limit that  $v_A^2 \gg c_s^2$ . As a result of this choice, the velocity perturbation is almost perfectly  $\parallel$  to the equilibrium magnetic field. The driving force is  $\parallel \delta \mathbf{F}_\perp$  and possesses a finite positive projection with the velocity perturbation  $\delta \mathbf{v}$ , allowing for the stratified background radiation field to perform work on the oscillating fluid.

in pressure due to temperature and neutrino chemical potential perturbations contribute to driving. Below the neutrinosphere, weak interactions occur so rapidly that the temperature and composition of the gas are dictated by the diffusive behavior of the neutrinos. With the help of eq. (99), the total driving force becomes

$$\delta\mathcal{F}_{\text{total}} = \frac{\hat{\mathbf{k}}}{c} \times \left[ \left( \frac{\partial P}{\partial T} \right)_{\rho, \mu_{\nu_e}} \frac{\kappa_{\text{eff}}}{\mathcal{K} k_B^2 T} \delta\mathbf{F}_Q + \left( \frac{\partial P}{\partial \mu_{\nu_e}} \right)_{\rho, T} \frac{\pi^2 \kappa_0}{\mathcal{K}} \delta\mathbf{F}_L \right]. \quad (103)$$

Both  $\delta\mathbf{F}_Q$  and  $\delta\mathbf{F}_L$  are  $\propto -\delta\rho/\rho$  implying that the perpendicular radiative fluxes reach their maximum possible upward values during density minima. Upon expansion radiation from the equilibrium heat and lepton fluxes more readily leaks out perpendicular to the direction of wavefronts as to avoid regions of enhanced density. Due to magnetic tension, then fluid oscillates in part along  $\mathbf{B}$ , which in general has some projection  $\perp$  to the wavefronts. Thus, the radiative driving force and the fluid velocity may oscillate in phase for certain propagation directions, ultimately allowing driving to occur.

### 5.6. Estimates of Local Stability and Driving

We have shown that in the limit of rapid neutrino diffusion, magnetoacoustic waves can be radiatively driven by both a background  $\mathbf{F}_Q$  and  $\mathbf{F}_L$ . Likewise, the waves can be damped by radiative diffusion due to the conversion of work into heat when  $(\partial s/\partial\rho)_{T, \eta_e} < 0$  as well as the loss of lepton pressure as a parcel of gas de-leptonizes, which occurs as long as  $(\partial Y_L/\partial\rho)_{T, \eta_e} < 0$ . Clearly, the growth rate given by eq. (83) can be thought of as two distinct stability criteria, one arising from the transport of heat and one due to the transport of lepton number. Ignoring all geometric factors (which are not completely negligible) the ‘‘condition’’ for radiative driving due to heat transfer is roughly given by

$$F_Q \gtrsim \frac{\omega \tilde{\omega}^2}{k^3 v_A^2} P_b \simeq \frac{v_A^3}{c_i^3} P_b c_i, \quad (104)$$

while the condition for radiative driving which derives from lepton transport reads

$$F_L \gtrsim \frac{\omega \tilde{\omega}^2}{k^3 v_A^2} n Y_L \simeq \frac{v_A^3}{c_i^3} n Y_L c_i. \quad (105)$$

The above stability criteria apply for the slow mode (which always has a larger growth rate than the fast mode; BS03) in the limit that both  $v_A^2/c_i^2 \lesssim 1$  and the background pressure support is primarily provided by the entropy of the baryons, which happens to be the case near the neutrinosphere. The two conditions for instability can be reconciled by re-writing eq. (105) as

$$k_B T F_L \simeq Y_L F_Q \gtrsim \frac{v_A^3}{c_i^3} n k_B T Y_L c_i \longrightarrow F_Q \gtrsim \frac{v_A^3}{c_i^3} P_b c_i = \rho v_A^3. \quad (106)$$

Therefore, neutrino-driven magnetoacoustic instability can be summed up by this criterion for both transport processes.

Substituting input conditions appropriate for regions near the neutrinosphere yields the instability condition

$$\text{INSTABILITY} \quad \left( \frac{L_\nu}{10^{53} \text{erg s}^{-1}} \right) \left( \frac{30 \text{km}}{R_\nu} \right)^2 \left( \frac{\rho_\nu}{10^{11} \text{g cm}^{-3}} \right)^{1/2} \left( \frac{10^{15} \text{G}}{B} \right)^3 \gtrsim 10^{-1} \quad (107)$$

where  $L_\nu$ ,  $R_\nu$ , and  $\rho_\nu$  are the neutrino luminosity, radius of the neutrinosphere, and density at the neutrinosphere, respectively. The stability criteria given by eq. (83) indicates that for field strengths at and above the equipartition value such that  $B^2/8\pi \sim P_b$ , the Alfvén speed in the above stability criteria can be replaced by the isothermal gas sound speed  $c_i \sim (P_b/\rho)^{1/2}$ . The equipartition value of the magnetic field  $B_{\text{eq}}$  near the neutrinosphere is roughly given by

$$B_{\text{eq}} \simeq 2 \times 10^{15} \left( \frac{\rho}{10^{11} \text{g cm}^{-3}} \right)^{1/2} \left( \frac{T}{4 \text{MeV}} \right)^{1/2} \text{G}, \quad (108)$$

which can be thought of as the magnetic field’s limiting value for eq. (107) to be valid. Deeper in the star, the degeneracy pressure of both the baryons and electrons overwhelms the contribution from the baryons’ entropy and the Fermi energies of both the electrons and baryons, rather than temperature, will enter into eq. (108) yielding a larger sound speed and thus a larger  $B_{\text{eq}}$ .

Though the stability criteria for both lepton and entropy driving are roughly equivalent, their respective growth and damping rates are not. From eq. (83), we see that the driving rate  $\gamma_L$  originating from gradients in  $\mu_{\nu_e}$ , which are  $\propto \mathbf{F}_L$ , for the slow mode is approximated by

$$\begin{aligned} \gamma_L &\simeq \frac{1}{2} \frac{v_A}{c_i} \left( \frac{\partial P}{\partial \mu_{\nu_e}} \right)_{\rho, T} \frac{\pi^2 \kappa_0}{c_i \mathcal{K}} F_L = \frac{1}{2} \frac{v_A}{\rho c_i^2} \left( \frac{\partial P}{\partial \mu_{\nu_e}} \right)_{\rho, T} |\nabla \mu_{\nu_e}| \\ &\simeq \frac{1}{2} \frac{v_A}{c_i} \frac{P_L}{P} \frac{g}{c_i}. \end{aligned} \quad (109)$$

The factor  $P_L/P$ , where  $P_L$  is the lepton pressure, may not be entirely negligible near the neutrinosphere. The driving rate due to gradients in temperature  $\gamma_Q$ , mediated by  $\mathbf{F}_Q$ , can be estimated in a similar fashion

$$\begin{aligned} \gamma_Q &\simeq \frac{1}{2} \frac{v_A}{c_i} \left( \frac{\partial P}{\partial T} \right)_{\rho, \mu_{\nu_e}} \frac{\kappa_{\text{eff}}}{c_i \mathcal{K} k_B^2 T} F_Q = \frac{1}{2} \frac{v_A}{\rho c_i^2} \left( \frac{\partial P}{\partial T} \right)_{\rho, \mu_{\nu_e}} |\nabla T| \\ &\simeq \frac{1}{2} \frac{v_A}{c_i} \frac{P_b}{P} \frac{g}{c_i}, \end{aligned} \quad (110)$$

where  $P_b$  is the baryon pressure. Near the neutrinosphere,  $P_b \sim P$ , but  $P_L$  is certainly non-negligible. Noting that  $P_L \simeq P_e \sim (\eta_e/4) Y_e P_b$  indicates that if radiative driving is allowed to occur at relatively large depths, where the degenerate lepton pressure becomes formidable, then the neutrino bubble instability results primarily from lepton, rather than heat, transport.

In terms of equilibrium parameters near the neutrinosphere, the combined neutrino bubble growth rate  $\gamma_{\text{NB}} \equiv \gamma_L + \gamma_Q$  is approximately

$$\gamma_{\text{NB}} \simeq 10^3 \left( \frac{B}{10^{15} \text{ G}} \right) \left( \frac{4 \text{ MeV}}{T} \right) \left( \frac{10^{11} \text{ g cm}^{-3}}{\rho} \right)^{1/2} \left( \frac{g}{10^{13} \text{ cm s}^{-2}} \right) s^{-1}. \quad (111)$$

As in the case of the instability criteria eq. (107), the value of the magnetic field  $B$  in the slow mode growth rate possesses an upper limit whose value is given by eq. (108).

Let us summarize the results of this section. Near the neutrinosphere, the condition for local driving due to the presence of  $\mathbf{F}_Q$  and  $\mathbf{F}_L$  are roughly equivalent. This is true primarily because the neutrino chemical potential  $\mu_{\nu_e} \sim k_B T$ , which implies that the flux of leptons directly maps to the flux of heat modulo a factor that is  $\sim Y_L$ . Neutrino bubble instabilities can grow on millisecond timescales for strong magnetic field strengths, with growth times  $\gtrsim 1$  ms for equipartition magnetic fields. Driving due to the presence of  $\mathbf{F}_Q$  mostly likely dominates the driving near the neutrinosphere over the radiative driving provided by  $\mathbf{F}_L$ .

## 6. MONTE CARLO CALCULATION

Assuming that radiative driving occurs in the upper layers of a PNS, neutrino bubbles may then lead to substantial luminosity enhancements and large density fluctuations in strongly magnetized regions. In order to make quantitative statements regarding the non-linear outcome of the neutrino bubble instability, a theory of radiation-driven magnetoacoustic turbulence is required. To our knowledge, such a theory unfortunately does not exist. We speculate how the saturation amplitude may change for different values of the local magnetic field strength in §7.2 under the assumption that significant non-linearities occur even for gas pressure dominated equilibria.

In order to proceed, we approximate the effects of the neutrino bubble instability by artificially altering the neutrino opacity in a radial and angular cut surrounding the neutrinosphere at early times after bounce. By doing so, we capture the cumulative effect that we expect neutrino bubbles produce on the surface of a PNS. From this deformed stellar background, the emitted neutrino flux is simulated via a Monte Carlo calculation so that the level of asymmetry in the outgoing radiation beam can be estimated. The angular profile of the neutrino flux allows us to further estimate the magnitude of the instantaneous kick as well as the gravitational wave strain and r-process efficiency.

### 6.1. Numerical Inputs and Techniques

There are three ingredients that go into our numerical model of the neutrino bubble powered mechanism: atmospheric structure, parameterization of the neutrino bubble instability, and radiative transfer. We describe each of them below.

#### 6.1.1. Proto-neutron star structure

The PNS that we use in our simulation was born from a  $15M_\odot$  progenitor (s15s7b - Woosley & Weaver 1995). Collapse, bounce, and early contraction are evolved up to a time of 130 ms after bounce using a 1-dimensional core-collapse code (Herant et al. 1994; Fryer et al. 1999). To this point, we assume that the evolution of the star is spherically symmetric and neutrino bubble oscillations have not yet begun.

#### 6.1.2. Neutrino Bubbles as a modified opacity

In our stellar model, the onset of neutrino bubble instability introduces deviations from spherical symmetry. As discussed in §2.1, neutrino bubbles are driven in starspots above the convection zone, but below the neutrinosphere. Effectively, one can model the global radiation asymmetry due to potential luminosity enhancements in starspots by reducing the opacity in those regions while the star's hydrostatic structure remains the same. By doing so, optically thick neutrinos preferentially leak out towards these starspots, producing a cumulative asymmetry in the neutrino beam, which emulates the effect of the acoustic instability. If in *reality*, the neutrino bubble instability behaves as the photon bubble instability in the non-linear regime, then large density fluctuations occur and the radiation preferentially leaks out of the rarefied regions, locally enhancing the outgoing flux (Begelman 2001, Turner et al. 2004).<sup>10</sup>

The angular extent of a starspot is parameterized by a covering fraction  $\mathcal{C}$  and values for  $\mathcal{C}$  are taken to be from 0.01-0.1. The radial extent for a neutrino bubble-active starspot is parameterized by an inner- and outer-radius  $\mathcal{R}_{in}$  and  $\mathcal{R}_{out}$ , respectively. A largely phenomenological justification for these values was given in §2.1. Throughout the neutrino bubble-active region, we reduce the neutrino opacity by a factor  $f$ . This reduction in opacity crudely characterizes the potentially multi-dimensional saturated state of the neutrino bubble instability into a single parameter. A list of values for  $\mathcal{C}$ ,  $\mathcal{R}_{in}$ ,  $\mathcal{R}_{out}$ , and  $f$  that are employed in our calculations are given in Table 1.

<sup>10</sup> Drawing conclusions regarding neutrino bubble saturation in PNSs from work done on photon bubbles in luminous accretion flows is dangerous. Those authors considered radiation pressure dominated media with superstrong magnetic fields. For PNSs, the magnetic field is not superstrong and the radiation field is significantly sub-Eddington in neutrinos.

## 6.1.3. Neutrino Transport

We simulate the transport of neutrinos through our neutrino bubble-deformed PNS 130 ms after bounce via the Maverick Monte Carlo transport code (Hungerford et al. 2003). In our calculations, we make several simplifying assumptions. We only model the electron neutrinos  $\nu_e$ , while assuming that the asymmetry they experience is representative of all neutrino species. We also assume that the asymmetry in the neutrino emission remains the same for the entire phase of neutron star cooling, which will inevitably lead to an overestimate of the net asymmetry. With these caveats, we can then calculate the total momentum kick and gravitational wave signal based on the total energy emitted in neutrinos for our neutron star (for our model, the total energy emitted is roughly  $5 \times 10^{53}$  erg).

Neutrino/matter interactions are calculated using a simplified opacity given by (Janka 2001)

$$\kappa_a \approx \frac{3\alpha^2 + 1}{4} \frac{\sigma_0}{m_n} \frac{\langle \epsilon_{\nu_e}^2 \rangle}{(m_e c^2)^2} Y_n \quad (112)$$

and

$$\kappa_{sc} \approx \frac{5\alpha^2 + 1}{24} \frac{\sigma_0}{m_n} \frac{\langle \epsilon_{\nu_e}^2 \rangle}{(m_e c^2)^2} (Y_n + Y_p). \quad (113)$$

Here,  $\sigma_0 = 1.76 \times 10^{-44}$  cm<sup>2</sup> is the characteristic weak interaction cross section and  $\alpha$  is the vector coupling constant in the vacuum. The absorption opacity  $\kappa_a$  is due to electron capture and the scattering opacity  $\kappa_{sc}$  results from elastic scattering off of nucleons. Neutrino annihilation was not included as an opacity source since the annihilation cross section becomes vanishingly small near the neutrinosphere, when compared to other sources of opacity. This follows from the fact that neutrinos propagate almost purely radially.

Neutrino emission rates from electron capture and electron-positron annihilations are taken from the temperature and density dependent functions given by Colgate, Herant & Benz (1993) and the energy distribution for the emitted neutrinos is taken from a simplified functional fit to the Fermi-Dirac distribution, as described by Keil, Raffelt & Janka (2003). Emitted neutrino energies were sampled from their Fermi sea with a two step (inversion followed by rejection) sampling technique.

Using appropriate Monte Carlo estimators, we track the spatial distribution of neutrino energy deposition, luminosity with respect to polar angle, and the net neutrino momentum. Neutrino deposition is tallied in a 2D cylindrical grid with 88 radial and 176 vertical bins. The Monte Carlo estimator for this quantity is the sum of packet luminosity for all packets absorbed at cylindrical coordinate  $(r; z)$ . The neutrino packets have uniform luminosity weight, so the Monte Carlo noise associated with the calculated deposition is proportional to the packet luminosity times  $\sqrt{N(r; z)}$ , where  $N(r; z)$  is the number of packets absorbed at cylindrical coordinate  $(r; z)$ . A typical value for the noise is roughly 0.003%, though along the polar axis the noise is significantly higher as the sampled cylindrical volume drops to zero at small radii. This purely numerical effect can be seen as dips in the deposition profile along the poles (see

TABLE 1  
MONTE CARLO SIMULATIONS

| $\mathcal{C}$ | $f$  | $\mathcal{R}_{out}$<br>(km) | $\mathcal{R}_{in}$<br>(km) | $V_{kick}$<br>(km/s) | $\langle h_{TT} \rangle_e$<br>(10 kpc) |
|---------------|------|-----------------------------|----------------------------|----------------------|--|
| 0.0           | 1    | —                           | —                          | 100                  | 1.0E-20                                |
| 0.1           | 2    | 90                          | 50                         | 1675                 | 1.3E-19                                |
| 0.1           | 2    | 90                          | 60                         | 965                  |  |
| 0.1           | 1.33 | 90                          | 50                         | 700                  |  |
| 0.1           | 1.33 | 90                          | 60                         | 520                  |  |
| 0.1           | 1.11 | 90                          | 60                         | 350                  |  |
| 0.1           | 1.11 | 90                          | 60                         | 220                  |  |
| 0.05          | 2    | 90                          | 50                         | 890                  |  |
| 0.05          | 2    | 90                          | 60                         | 530                  | 5.E-20                                 |
| 0.01          | 2    | 90                          | 50                         | 175                  |  |
| 0.01          | 2    | 90                          | 60                         | 120                  |  |
| 0.1           | 2    | 120                         | 50                         | 2350                 |  |
| 0.1           | 2    | 120                         | 60                         | 1500                 |  |
| 0.1           | 1.33 | 120                         | 50                         | 950                  |  |
| 0.1           | 1.33 | 120                         | 60                         | 700                  |  |
| 0.05          | 2    | 120                         | 50                         | 1250                 |  |
| 0.05          | 2    | 120                         | 60                         | 800                  |  |
| 0.01          | 2    | 120                         | 50                         | 250                  |  |
| 0.01          | 2    | 120                         | 60                         | 200                  |  |



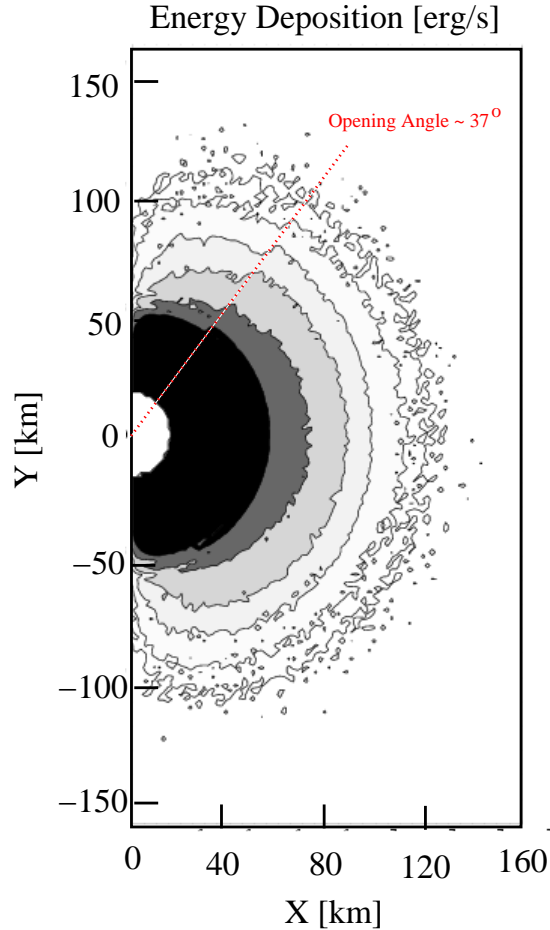


FIG. 3.— Neutrino energy deposition contours for  $C = 0.1$ ,  $f = 2$ ,  $\mathcal{R}_{out} = 120$  km,  $\mathcal{R}_{in} = 50$  km. Contour levels plotted are 0.06, 0.2, 0.8, 2.2, 7 and 27 in units of  $10^{50} \text{ergs s}^{-1}$ . Note that the contours move inward slightly over the cone of lower opacity (cone opening angle is roughly  $37^\circ$  for  $C = 0.1$ ). This slight deviation from spherical symmetry will not likely cause strong variations in the PNS wind. The decrease in deposited energy right along the symmetry axis is the result of insufficient sampling due to the smaller volume at small radii.

Figure 3). Note that numerical noise is given in terms of energy per unit time since we are only considering a short time-slice in the evolution of the PNS.

The angular distribution of the neutrino luminosity is similarly calculated by summing the luminosity of escaping neutrino packets into 11 angular bins along the polar direction. For a given bin direction  $\theta$ , packets escaping with direction  $\theta \pm \Delta\theta$  are counted in the sum (where  $\Delta\theta = 2.5^\circ$ ). As before, the noise goes as the packet luminosity times  $\sqrt{N(\theta)}$ , where  $N(\theta)$  is the number of packets in angular bin  $\theta$ , which works out to be roughly 0.01% (see Figure 3). The Monte Carlo estimator for net neutrino momentum is given, in component form ( $p_x$ ,  $p_y$  and  $p_z$ ), by

$$p_x = \sum_0^{N_{esc}} \frac{L_{pckt}}{c} \times \mu_x; \quad p_y = \sum_0^{N_{esc}} \frac{L_{pckt}}{c} \times \mu_y; \quad p_z = \sum_0^{N_{esc}} \frac{L_{pckt}}{c} \times \mu_z, \quad (114)$$

where  $N_{esc}$  is the number of escaped packets,  $L_{pckt}$  is the weight of the packet in units of luminosity,  $c$  is the speed of light and  $\mu_x, \mu_y, \mu_z$  are the direction cosines with respect to the coordinate axes. This is the most well determined quantity from these simulations, as it is tabulated from all escaping neutrino packets ( $N_{esc} \approx 2 \times 10^6$ ). The uncertainty in the net neutrino momentum per unit time resulting from angular discretization is of order  $10^{40} \text{gcm s}^{-2}$ . As the first line of Table 1 shows, numerical noise alone is responsible for momentum asymmetries in our calculations, leading to velocity kicks  $\sim 100 \text{km s}^{-1}$  if this artificial asymmetry were to continuously discharge its momentum onto the star for  $\sim 1$  s.

## 6.2. Numerical Results

Now we are in the position to provide estimates of the kick imparted, r-process yields, and gravitational wave strains which may result from the neutrino bubble instability. Values for these observable quantities are provided in Table 1.

Our work focuses on the origin of neutron star kicks, which is the most dramatic effect of neutrino bubble instability on the core-collapse environment. The total momentum carried away by the neutrinos in the collapse is equal to the total neutrino energy emitted divided by the speed of light. The asymmetry in neutrino emission carries away a net linear momentum. The total asymmetry is measured at infinity rather than at the neutrinosphere. Thus, the optically thin matter above the region of neutrino bubble instability reduces the asymmetry by a multiplicative factor  $\sim e^{\tau_\nu}$  and most likely leads to an underestimate of the momentum kick. As expected, Table 1 shows that neutrino bubbles may drive kicks in excess of  $1000 \text{ km s}^{-1}$ . We assume that the kick is discharged for  $\sim 1 \text{ s}$ , which can be thought of as the best case scenario. Further, we are implicitly assuming that the spin and the starspot are exactly aligned. This assumption overestimates the kick by the value of the cosine of the angle between the spin axis and the starspot.

In order for neutrino bubbles to affect the r-process or the supernova explosion, it need not alter the total energy deposition of neutrinos dramatically, but it must induce an asymmetry in this deposition. Our simulations show that this instability produces only a small asymmetry, and the total heating from the proto-neutron star is essentially spherically symmetric, even for our most extreme case (see Figure 3).

However, these small asymmetries may lead to large differences in the gravitational wave output and spectrum. The gravitational wave amplitude ( $h_{xx}^{\text{TT}}$ ) for an observer orthogonal to the symmetry axis for asymmetric neutrino emission is given by (Müller & Janka 1997; Fryer et al. 2004):

$$(h_{xx}^{\text{TT}})_{\text{pole}} = \frac{2G}{c^4 R} \sum \Delta t \sum_{p=1}^N (1+z/r)(2x^2/r^2 - 1) \Delta L_\nu. \quad (115)$$

The neutrino luminosity,  $\Delta L_\nu$ , at a position  $x, y, z$  ( $r = (x^2 + y^2 + z^2)^{1/2}$ ) over a given time ( $\Delta t$ ) must be summed over all time to give the total wave amplitude. For our suite of models, the gravitational wave amplitude (assuming the asymmetry persists for 1 s) is sufficiently high to be detectable by advanced LIGO observing a Galactic supernova.<sup>11</sup> Although this signal will be very different than the gravitational wave signal from rotating supernovae, it will not be dramatically different from other asymmetries in supernovae (e.g. asymmetric collapse - Burrows & Hayes 1996; Fryer 2004).

## 7. UNCERTAINTIES, COMPARISON WITH OTHER KICK MECHANISMS, AND FUTURE WORK

The neutrino bubble powered kick mechanism presented here is subject to several uncertainties, many of which have not been mentioned thus far. In what follows, we assess its major weaknesses and by doing so, provide motivation for future work.

### 7.1. Global Stability

We have focused on the physics of *local* magnetoacoustic stability in the presence of a stratified degenerate optically thick radiation field. We can not stress enough, that drawing conclusions regarding stability from a local linear analysis is dangerous at best. In order to confirm that neutrino bubbles are important in PNSs, a *global* analysis must be performed using a full non-adiabatic treatment since the region of greatest driving lies near the neutrinosphere, where the radiative diffusion time is short in comparison to the acoustic crossing time. Our kick model requires a magnetic field that perhaps originates from vigorous convective motion beneath the upper radiative layer. Turbulent motions almost certainly reduce the driving rate of a given trapped wave (Goldreich & Keeley 1977). However, even if the interaction between a mode and turbulence is accurately quantified, calculating the cumulative damping rate throughout the run of the star requires knowledge of the mode's profile as a function of depth.

### 7.2. Saturation Amplitude

Assuming that one finds trapped neutrino bubble oscillations in a global eigenmode calculation, computing the saturation amplitude is a much more difficult task since a fully non-linear degenerate radiation magnetohydrodynamic analysis is required. But, from a computational expense point of view, the situation may not be as costly as in the case of main sequence stars and the accretion disks that are thought to power active galactic nuclei and X-ray binaries. Since the sound speed is relatively close to the speed of light in PNSs, the ratio of the sound crossing time to the radiation diffusion time near the surface of last scattering is only a factor of  $\sim 30$  or so. For the A-star discussed in §2, this ratio is  $\sim 10^4$ .

We expect that the saturation amplitude becomes smaller for decreasing values of the magnetic field strength. If the saturation amplitude depends on the ratio of equilibrium magnetic to gas pressure evaluated at the neutrinosphere, then large flux enhancements would not occur for local field strengths  $< 10^{15} \text{ G}$ . However, if the saturation amplitude varies with respect to the ratio of the Alfvén speed  $v_A$  to the gas sound speed  $c_i$ , then perhaps field strengths of order  $\sim$  a few times  $10^{14} \text{ G}$  may lead to a saturation amplitude of order  $v_A/c_i \sim 1/3$ . Of course, the entire kick model relies on the fact that significant luminosity enhancements are reached for thermally- and chemically-locked perturbations in gas pressure dominated media. The results of §§4, 5, and of BS03 inform us that dynamical growth rates can be achieved for wavelengths of order the gas pressure scale height (where our WKB analysis breaks down). Therefore, the energy injected into the mode by the instability is comparable to the kinetic energy of the mode itself. Whether or not this leads to order unity saturation amplitudes is a question that can only be answered with confidence by a careful non-linear analysis.

### 7.3. Magnetic Field Structure

The neutrino bubble instability can not power a kick unless strong magnetic structures, with length scales significantly larger than the gas pressure scale height at the neutrinosphere, are maintained for hundreds of convective overturn times. Reasons for believing

<sup>11</sup> Depending upon the duration of the explosion, the neutrino luminosity can vary considerably over this 1 s time period and it is possible that the gravitational wave amplitude may be even higher (perhaps lower) than this predicted value, but this value gives a rough estimate of the expected signal.

that such fields exist in young PNSs were given in §2.1. Our arguments regarding magnetic field structure were primarily based on phenomenological arguments derived from the Sun. However, even after the discovery of the solar tachocline (Goode et al. 1991) and the understanding of its importance with respect to magnetic field generation (Spiegel & Zahn 1992), the evolution of the Sun’s surface magnetic field throughout the solar convection zone evades a coherent theoretical picture. Numerical simulations of PNS magnetic field structure may prove to be more fruitful than those of their main sequence counterparts since a PNS convection zone encompasses relatively few gas pressure scale heights in comparison to say, the solar convection zone.

#### 7.4. Handling of the Neutrino Transport

We have ignored the compositional dependence of the neutrino opacities in our linear analysis. Not only does this change the numerical value of the opacity, but more importantly, we may have overlooked certain instability phenomena as well. In general, the neutrino absorption opacity depends on the proton fraction (see eq. (112) and Janka 2001). Since the proton fraction  $Y_p$  depends on fluid’s density, the opacity perturbation  $\delta\kappa$  varies with the density perturbation  $\delta\rho$  implying that standard hydrodynamic sound waves which display some degree of radial propagation can be driven unstable by the presence of the radiative fluxes (Unno et al. 1989, Glatzel 1994, BS03). Therefore, when the compositional variation of the absorption opacity is taken into account,  $\kappa$ -mechanism and strange mode phenomena may ensue on the entire surface of the proto neutron star i.e., radiative driving occurs in un-magnetized regions as well. If thermal locking holds, the growth rate near the neutrinosphere from local radiative driving is comparable to that given by the upper limit of eq. (111). Certainly, if the  $\kappa$ -mechanism or strange mode instability occurs at early times, luminosity perturbations of only  $\sim 10\%$  could play an important role with respect to shock ejection and the overall explosion mechanism. Fully understanding how this different instability phenomenon affects the neutrino bubble kick mechanism requires answering the questions posed by §§7.1-7.3.

#### 7.5. Comparison with Other Kick Mechanisms

If these theoretical hurdles are overcome, a neutrino bubble powered kick mechanism possesses attractive differences when compared to other mechanisms. In order to obtain spin-kick alignment, as is seen in the Crab and Vela systems, the impulse must be imparted on timescales significantly in excess of the rotation period (Lai, Cordes, & Chernoff 2001). In “mass-rocket” models, a PNS receives various impulses with durations of order  $\sim$  a few milliseconds each (Burrows & Hayes 1996; Lai & Goldreich 2000; Fryer 2004). Therefore, spin-kick alignment most likely does not follow from the hydrodynamic mass-rocket mechanism unless the initial rotation period is  $\lesssim$  a millisecond. However, this fact only rules out the mass-rocket model for the Crab and Vela systems, which may not be representative of the Galactic pulsar distribution. Fryer (2004) argues that the mass-rocket works only for rapid explosions so that the convective motions in the gain region do not have enough time to damp out the mean motion of the PNS. Therefore, mass-rocket kick models are heavily prejudiced towards neutron stars born from progenitors with mass  $< 12M_\odot$ .

Recently, another hydrodynamic powered kick model that depends on delayed explosions triggering global Rayleigh-Taylor instability has been further elaborated by way of detailed numerical simulation (Scheck et al. 2004). Their model requires the stellar neutrino emission to be somewhat uniformly discharged over the first second so that the refreshment epoch is prolonged. This allows global Rayleigh-Taylor type instability to develop beneath the shock front since the density and pressure gradients lie in the opposite direction across the shock (Thompson 2000, Herant 1995). A prolonged refreshment is necessary in order to allow the lowest order ( $l = 1, 2$ ) modes to dominate the non-linear phase. This mechanism does not lead to spin-kick alignment and most likely requires weak explosions.

The parity violation model of Arras & Lai (1999a, 1999b) naturally produces spin-kick alignment as do all neutrino-powered kick mechanisms. This results from the basic fact that the Kelvin-Helmholtz time, which is the discharge timescale for neutrino powered kicks, is most likely much longer than the rotation period. Also, neutrino-driven kick mechanisms are not subject to convective damping in the gain region as in the case of the mass-rocket mechanism since the the shell of accreting material beneath the outgoing shock can easily adjust its center of mass to that of the kicked PNS. As previously mentioned, the parity-violation mechanism requires global magnetic flux densities  $\sim 10^{16}$  G, a large value even for magnetars. Say for example, that the neutrino bubble powered kick mechanism requires flux densities of comparable strength in order to produce order unity luminosity enhancements over a starspot. Then, such a starspot would only need to cover  $\sim 10\%$  of a hemisphere. Thus, the total amount of flux necessary for the neutrino bubble mechanism, for this rather extreme case, is  $\sim 10\%$  of that required for the parity violation model. In terms of the overall magnetic energy budget, the neutrino bubble mechanism requires  $\sim 1\%$  of the total magnetic energy with respect to the parity violation model.

There may not be a single explanation for neutron star kicks. Perhaps all, some, or none of the kick mechanisms mentioned here (including ours) work for different classes of progenitors. The best way to differentiate between the various kick mechanisms is to constrain models with observations and analysis of the Galactic pulsar and neutron star population. For example, determining the fraction of systems which possess spin-kick alignment, quantifying the robustness of the inferred bimodal distribution as well as the correlation between kick velocity and magnetic field strength will help constrain the applicability of these various mechanisms.

We thank P. Arras, L. Bildsten, A. Burrows, P. Chang, B. Pacynski, R. Rosner, C. Thompson, and N. Turner for enlightening conversations regarding a variety of topics. This work was supported by Los Alamos National Laboratory/UCSB CARE grant SBB-001A, and NASA grant NAG5-13228. A portion of this work was also funded under the auspices of the U.S. Department of Energy through contract W-7405-ENG-36 to Los Alamos National Laboratory. The simulations were conducted on Space Simulator at Los Alamos National Laboratory. A.S. acknowledges financial support from a Hubble Fellowship administered by the Space Telescope Science Institute.

## REFERENCES

- Arons, J. 1992, ApJ, 388, 561  
 Arras, P. & Lai, D. 1999a, ApJ, 519, 745  
 Arras, P. & Lai, D. 1999b, PhRvD, 60, 3001  
 Arzoumanian, Z., Chernoff, D.F., & Cordes, J.M. 2002, ApJ, 568, 289  
 Baker, N. & Kippenhahn, R. 1962, ZA, 54, 114  
 Begelman, M.C. 2001, ApJ, 376, 214  
 Bethe, H.A., Brown, G. E., & Cooperstein, J. 1987, ApJ, 322, 201  
 Bludman, S.A. & van Riper, K.A. 1978, ApJ, 224, 631  
 Bruenn, S.W. & Dineva, T. 1996, 458, L71  
 Bruenn, S.W., Raley, E.A., & Mezzacappa, A. 2004, astro-ph/0404099  
 Blaes, O.M. & Socrates, A. 2003, ApJ, 596, 509 BS03  
 Burrows, A. & Lattimer, J.M. 1986, ApJ, 307, 178  
 Burrows, A., Mazurek, T.J., & Lattimer, J.M. 1981, ApJ, 251, 325  
 Burrows, A., & Hayes, J. 1996, PRL, 76, 352  
 Cattaneo, F., & Vainshtein, S.I. 1991, ApJ, 376, L21  
 Colgate, S. A., Herant, M., & Benz, W. 1993, Physics Reports, 227, 157  
 Cordes, J.M., & Chernoff, D.F. 1998, ApJ, 505, 315  
 Duncan, R.C., & Thompson, C. 1992, ApJ, 392, L9  
 Fryer, C. L. 2004, ApJ, 601, L175  
 Fryer, C., Benz, W., Herant, M., & Colgate, S. A. 1999, ApJ, 516, 892  
 Fryer, C., Burrows, A., & Benz, W. 1998, ApJ, 496, 333  
 Fryer, C. L., Holz, D. E., & Hughes, S. A. 2004, 609, 288  
 Fryer, C.L., & Kalogera, V. 1997, ApJ, 489, 244  
 Gammie, C.F., 1998 MNRAS, 297, 929  
 Glatzel, W. 1994, MNRAS, 271, 66  
 Goldreich, P., & Keeley, D.A. 1977, ApJ, 211, 934  
 Goldreich, P., Murray, N., Willette, G., & Kumar, P. 1991, ApJ, 370, 752  
 Goode, P.R., Dziembowski, W.A., Korzennik, S.G., Rhodes, E.J., 1991, ApJ, 367, 649  
 Gunn, J.E. & Ostriker, J.P. 1970, ApJ, 160, 979  
 Herant, M. 1995, Phys. Reports, 256, 117  
 Herant, M., Benz, W., Hix, W. R., Fryer, C. L., Colgate, S. A. 1994, ApJ, 435, 339  
 Hungerford, A. L., Fryer, C. L., & Warren, M. S. 2003, ApJ, 594, 390  
 Janka, H.-T., 1991, A&A, 244, 378  
 Janka, H.-T., 2001, A&A, 368, 527  
 Keil, W., Janka, H.-T., & Müller, E. 1996, ApJ, 473, L111 KJM96  
 Keil, M. T., Raffelt, G. G., & Janka, H.-T. 2003, ApJ, 590, 971  
 Kramer, M. 1998, ApJ, 509, 856  
 Lai, D., Chernoff, D.F., & Cordes, J.M. 2001, ApJ, 549, 1111  
 Lai, D., & Goldreich, P. 2000, ApJ, 535, 402  
 Lai, D. & Qian, Y.-Z. 1998, astro-ph/9802345  
 Libbrecht, K.G. & Woodard, M. F. 1990, Nature, 345, 779  
 Lorimer, D.R., Bailes, M., & Harrison, P.A. 1993, MNRAS, 263, 403  
 Lucy, L.B. 1982, ApJ, 255, 286L  
 Lucy, L.B., & White, R.L. 1980, ApJ, 241, 300L  
 Lyne, A.G., & Lorimer, D.R. 1994, Nature, 369, 127  
 Mirabel, I.F., Mignani, R., Rodrigues, I., Combi, J.A., Rodríguez, L.F., & Guglielmetti, F. 2002, 2002, A&A, 395, 595  
 Miralles, J.A., Pons, J.A., Urpin, V.A. 2000, ApJ, 543, 1001  
 Müller, E. & Janka, H.-T. 1997, A&A, 317, 140  
 Pathria, R.K. 1996, Statistical Mechanics (Oxford: Butterworth-Heinemann)  
 Pons, J.A. et al. 1999, ApJ, 513, 780  
 Scheck, L., Plewa, T., Janka, H.-T., Kifonidis, K., & Müller, E. 2004, Phys. Rev. Lett., 92, 1103  
 Schrijver, C.J., Title, A.M., van Ballegooijen, A.A., Hagenaar, H.J., & Shine, R.A. 1987, ApJ, 487, 424  
 Silk, J. 1968, ApJ, 151, 459  
 Spiegel, E.A., Zahn, J.-P. 1992, A&A, 265, 106  
 Stenflo, J.O. 1989, A&ARv, 1, 3  
 Tauris, T.M., Fender, R.P., van den Heuvel, E.P.J., Johnston, H.M., & Wu, K. 1999, MNRAS, 310, 1165  
 Thompson, C. 2000, ApJ, 534, 915  
 Thompson, C. & Duncan, R.C. 1993, ApJ, 408, 194  
 Thompson, C. & Murray, N. 2001, ApJ, 560, 339  
 Tobias, S.M., Brummel, N.H., Clune, T.L., & Toomre, J. 1998, ApJ, 502, L177  
 Tobias, S.M., Brummel, N.H., Clune, T.L., & Toomre, J. 2001, ApJ, 549, 1183  
 Turner, N., Blaes, O., Socrates, A., Begelman, M.C., David, S.W. 2004, ApJ submitted  
 Unno, W., Osaki, Y., Ando, H., Saio, H., Shibahashi, H. 1989, Nonradial Oscillations of Stars (Tokyo: University of Tokyo Press)  
 Wex, N., Kalogera, V., & Kramer, M. 2000, ApJ, 528, 401  
 Woosley, S. E., Weaver, T. A. 1995, ApJS, 101, 181

## APPENDIX

## APPENDIX A: THERMODYNAMIC QUANTITIES AND RELATIONS

Here, we derive the expressions for the neutrino energy and lepton flux as well as other important thermodynamic quantities. Much of this Appendix is covered by Bludman & Van Riper (1978) as well as Lai & Qian (1998).

All spin 1/2 particle species are assumed to possess a Fermi-Dirac distribution  $f$  where

$$f_i = \frac{1}{e^{(E-\mu_i)/k_B T} + 1} \quad (\text{A1})$$

for the  $i^{\text{th}}$  species. Thus, any given particle distribution is parameterized solely by a temperature and chemical potential, both of which vary as a function of depth. In the diffusion approximation the energy density, number density, energy flux, and particle flux are given by

$$U = \int dE U_E = \int dE \frac{4\pi}{h^3 c^3} E^3 f, \quad n = \int dE \frac{U_E}{E}, \quad \mathbf{F} = -\frac{c}{3\rho} \int dE \frac{1}{\kappa(E)} \nabla U_E, \quad \text{and} \quad \mathbf{H} = -\frac{c}{3\rho} \int dE \frac{1}{\kappa(E)} \nabla \frac{U_E}{E} \quad (\text{A2})$$

respectively. For sake of simplicity, we assume that  $\kappa(E)$  depends solely on energy as given by eq. (5) and is the sum of both the scattering and absorption opacities. Integrating over energy we obtain

$$U = \frac{k_B^4 T^4}{2\pi^2 \hbar^3 c^3} F_3(\eta), \quad n = \frac{k_B^3 T^3}{2\pi^2 \hbar^3 c^3} F_2(\eta), \quad \mathbf{F} = -\frac{E_0^2 k_B^2}{6\pi^2 \kappa_0 \rho \hbar^2 c^2} \nabla [T^2 F_1(\eta)], \quad \text{and} \quad \mathbf{H} = -\frac{E_0^2 k_B}{6\pi^2 \kappa_0 \rho \hbar^2 c^2} \nabla [T F_0(\eta)] \quad (\text{A3})$$

where  $F_n(\eta)$  is the standard Fermi-Dirac integral given by

$$F_n(\eta) = \int_0^\infty dx \frac{x^n}{e^{x-\eta} + 1}. \quad (\text{A4})$$

The chemical potential of the electron-type neutrinos obey the relation  $\mu_{\nu_e} = -\mu_{\bar{\nu}_e}$  which allows us to write

$$U_{\nu_e} + U_{\bar{\nu}_e} = \frac{7\pi^2 k_B^4 T^4}{120 \hbar^3 c^3} \left[ 1 + \frac{30}{7} \left( \frac{\eta_{\nu_e}}{\pi} \right)^2 + \frac{15}{7} \left( \frac{\eta_{\nu_e}}{\pi} \right)^4 \right], \quad (\text{A5})$$

$$Y_{\nu_e} = \frac{n_{\nu_e} - n_{\bar{\nu}_e}}{n} = \frac{k_B^3 T^3}{6n \hbar^3 c^3} \eta_{\nu_e} \left( 1 + \frac{\eta_{\nu_e}^2}{\pi^2} \right), \quad (\text{A6})$$

$$\mathbf{F}_{\nu_e} + \mathbf{F}_{\bar{\nu}_e} = -\frac{E_0^2 k_B^2}{6\pi^2 \kappa_0 \rho \hbar^3 c^2} \nabla \left[ T^2 \left( \frac{\eta_{\nu_e}^2}{2} + \frac{\pi^2}{6} \right) \right], \quad (\text{A7})$$

and

$$\mathbf{F}_L = \mathbf{H}_{\nu_e} - \mathbf{H}_{\bar{\nu}_e} = -\frac{E_0^2 k_B}{6\pi^2 \kappa_0 \rho \hbar^2 c^2} \nabla [T \eta_{\nu_e}]. \quad (\text{A8})$$

The lepton flux,  $\mathbf{F}_L$ , is solely carried by the electron- type neutrinos due to their macroscopic mean free paths and because the  $X$ -type neutrinos are produced only from pair annihilation processes. The above relations were obtained with the help of the following expressions (Bludman & Van Riper 1978)

$$\begin{aligned} F_0(\eta) - F_0(-\eta) &= \eta \\ F_1(\eta) + F_1(-\eta) &= \frac{\eta^2}{2} + \frac{\pi^2}{6} \\ F_2(\eta) - F_2(-\eta) &= \frac{\eta}{3} [\eta^2 + \pi^2] \\ F_3(\eta) + F_3(-\eta) &= \frac{7\pi^4}{60} + \frac{1}{2} \eta^2 \left[ \pi^2 + \frac{1}{2} \eta^2 \right]. \end{aligned} \quad (\text{A9})$$

The number densities, energy densities, and fluxes for all other fermionic species (pairs and  $X$ -type neutrinos) can be quickly obtained repeating the procedure outlined above.

#### APPENDIX B: CONDITIONS FOR SILK DAMPING, DIFFUSIVE HEATING, AND DAMPING FROM LEPTON PRESSURE LOSS

In order to see if diffusive heating occurs at all for short wave-length compressible waves, the ‘‘Silk determinant’’ must be greater than zero i.e.,

$$nT \left( \frac{\partial s}{\partial \rho} \right)_{T, \mu_{\nu_e}} = \left( \frac{\partial U}{\partial \rho} \right)_{T, \mu_e} - \frac{U+P}{\rho} - \mu_{\nu_e} n \left( \frac{\partial Y_L}{\partial \rho} \right)_{T, \mu_{\nu_e}} > 0. \quad (\text{B1})$$

In order to evaluate this expression, we need to specify an equation of state. Photons and leptons obey relativistic equations of state for bosons and fermions, respectively. However, the quantum mechanical behavior for the non-relativistic baryons varies with increasing depth. In the inner and outer core, the baryons are mildly degenerate, while near the neutrinosphere baryons behave as a classical ideal gas ( $P \propto nT$ ).

It is convenient to define a fiducial Fermi energy for the non-relativistic baryons

$$\epsilon_F \equiv \frac{\hbar^2}{2m_n} p_F^2 = \frac{\hbar^2}{2m_n} (3\pi^2 n)^{2/3} \simeq 124 \rho_{15}^{2/3} \text{MeV} \quad (\text{B2})$$

such that the Fermi energy and zero-point pressure for the neutrons and protons can be conveniently written as

$$\epsilon_{n,p} \equiv Y_{n,p}^{2/3} \epsilon_F \quad \text{and} \quad P_{n,p}^{(0)} = \frac{2}{3} U_{n,p}^{(0)} = \frac{2}{5} Y_{n,p}^{5/3} n \epsilon_F \quad (\text{B3})$$

respectively. At early times in the mantle and near the neutrinosphere,  $\epsilon_F \simeq 6 \rho_{12}^{2/3} \text{MeV}$  while  $k_B T \simeq 10 - 30 \text{MeV}$  such that the contribution to the baryon pressure arising from degeneracy may be neglected at first approximation. Deep in the core below the mantle, the degeneracy pressure of the baryons is substantial such that  $\epsilon_{n,p} \sim Y_{n,p}^{2/3} 60 \text{MeV}$  is significantly larger than  $k_B T \simeq 15 - 20 \text{MeV}$  (Pons et al. 1999). Their pressure is approximately given by

$$P_{n,p} \simeq P_{n,p}^{(0)} \left[ 1 + \frac{5\pi^2}{12 Y_{n,p}^{4/3}} \left( \frac{k_B T}{\epsilon_F} \right)^2 \right] \quad (\text{B4})$$

where we have kept the substantial finite temperature contribution for each baryonic species. The only species significantly contributing to the first term in eq. (B1) are the neutrons and electrons where

$$\left( \frac{\partial U_n}{\partial \rho} \right)_{T, \mu_e} = \left( \frac{\partial U_n}{\partial \rho} \right)_{T, \mu_e, \mu_{\nu_e}} + \left( \frac{\partial \mu_e}{\partial \rho} \right)_{T, \mu_{\nu_e}} \left( \frac{\partial U_n}{\partial \mu_e} \right)_{\rho, T, \mu_{\nu_e}} \simeq \frac{5}{3} \frac{U_n^{(0)}}{Y_n} \frac{1}{\rho} \left[ 1 + \frac{5\pi^2}{12 Y_n^{4/3}} \left( \frac{k_B T}{\epsilon_F} \right)^2 \right] - \frac{4}{3} \frac{U_n^{(0)}}{Y_n} \frac{5\pi^2}{12 Y_n^{4/3}} \left( \frac{k_B T}{\epsilon_F} \right)^2 \quad (\text{B5})$$

$$\left( \frac{\partial U_e}{\partial \rho} \right)_{T, \mu_{\nu_e}} = \left( \frac{\partial \mu_e}{\partial \rho} \right)_{T, \mu_{\nu_e}} \left( \frac{\partial U_e}{\partial \mu_e} \right)_{\rho, T, \mu_{\nu_e}} \simeq \frac{3 Y_e}{Y_n} \frac{k_B T}{m_n}. \quad (\text{B6})$$

Terms  $\mathcal{O}(k_B T / \mu_e)$  have been dropped for the sake of simplicity, which is why the proton contribution has been neglected. This is not a bad approximation during early times throughout the core where  $\mu_e / k_B T \sim 10 - 20$  (Burrows & Lattimer 1986, Pons et al. 1999).

The last term in eq. (B1), which is largely responsible for diffusive heating of compressible perturbations is given by

$$-\mu_{\nu_e} n \left( \frac{\partial Y_L}{\partial \rho} \right)_{T, \mu_{\nu_e}} = -\mu_{\nu_e} n \left[ \left( \frac{\partial Y_L}{\partial \rho} \right)_{T, \mu_e, \mu_{\nu_e}} + \left( \frac{\partial \mu_e}{\partial \rho} \right)_{T, \mu_{\nu_e}} \left( \frac{\partial Y_L}{\partial \mu_e} \right)_{\rho, T, \mu_{\nu_e}} \right] \simeq + \frac{\mu_{\nu_e}}{m_n} Y_L. \quad (\text{B7})$$

Thus, to  $\mathcal{O}(k_B T / \mu_e)$  the Silk determinant is given by

$$\begin{aligned} nT \left( \frac{\partial s}{\partial \rho} \right)_{T, \mu_{\nu_e}} &\simeq \frac{5 Y_p}{3 Y_n} \frac{U_n^{(0)}}{\rho} \left[ 1 + \frac{5\pi^2}{12 Y_n^{4/3}} \left( \frac{k_B T}{\epsilon_F} \right)^2 \right] - \frac{4}{3} \frac{U_n^{(0)}}{Y_n} \frac{5\pi^2}{12 Y_n^{4/3}} \left( \frac{k_B T}{\epsilon_F} \right)^2 + \frac{3 Y_e}{Y_n} \frac{k_B T}{m_n} \\ &\quad - \frac{5 U_p^{(0)}}{3} \frac{1}{\rho} \left[ 1 + \frac{5\pi^2}{12 Y_p^{4/3}} \left( \frac{k_B T}{\epsilon_F} \right)^2 \right] - \frac{\mu_e}{m_n} Y_e - \frac{\mu_{\nu_e}}{m_n} Y_{\nu_e} + \frac{\mu_{\nu_e}}{m_n} Y_L. \end{aligned} \quad (\text{B8})$$



By putting in typical values for the core ( $Y_n \sim 0.7$ ,  $Y_L \sim 0.34$ ,  $\epsilon_F \sim 60$  MeV,  $k_B T \sim 20$  MeV,  $\mu_e - \mu_{\nu_e} \sim 30$  MeV) the Silk determinant is approximately given by

$$nT \left( \frac{\partial s}{\partial \rho} \right)_{T, \mu_{\nu_e}} \simeq \frac{5 - 10 \text{ MeV}}{m_n}, \quad (\text{B9})$$

which of course, is greater than zero. In order to realistically assess this result, we must note that the typical energy scales in this problem are given by the thermal energy per particle  $k_B T \sim 20$  MeV and the Fermi energy  $\epsilon_F \sim 60$  MeV. Quantitatively, the value of the Silk determinant given above is obtained by adding and subtracting characteristic energies of order  $\sim 20 - 60$  MeV. Therefore, the answer given by eq. (B9) should be taken with extreme caution and a more careful calculation is necessarily required.

Even though the Silk determinant is positive, a given compressible wave is not necessarily driven. Unstable driving from the entropy perturbation must overcome the loss of degeneracy pressure due to lepton diffusion during compression. From the form of the pressure perturbation given by eq. (56) or equivalently from the asymptotic growth rate given eq. (83), Silk driving or diffusive heating will occur if

$$\frac{\kappa_{\text{eff}}}{k_B^2 T} \left( \frac{\partial P}{\partial T} \right)_{\rho, \mu_{\nu_e}} nT \left( \frac{\partial s}{\partial \rho} \right)_{T, \mu_{\nu_e}} + \pi^2 \kappa_0 \left( \frac{\partial P}{\partial \mu_{\nu_e}} \right)_{\rho, \mu_{\nu_e}} n \left( \frac{\partial Y_L}{\partial \rho} \right)_{T, \mu_{\nu_e}} > 0. \quad (\text{B10})$$

Derivatives of the total pressure with respect to temperature and neutrino chemical potential are approximately given by

$$\left( \frac{\partial P}{\partial T} \right)_{\rho, \mu_{\nu_e}} = \left( \frac{\partial P}{\partial T} \right)_{\rho, \mu_e, \mu_{\nu_e}} + \left( \frac{\partial \mu_e}{\partial T} \right)_{\rho, \mu_{\nu_e}} \left( \frac{\partial P}{\partial \mu_e} \right)_{\rho, T, \mu_{\nu_e}} \simeq \frac{\pi^2}{3} \left( \frac{k_B T}{\epsilon_F} \right) n k_B \left[ Y_n^{1/3} + Y_p^{1/3} \right] + n k_B Y_e, \quad (\text{B11})$$

$$\left( \frac{\partial P}{\partial \mu_{\nu_e}} \right)_{\rho, T} = \left( \frac{\partial P}{\partial \mu_{\nu_e}} \right)_{\rho, T, \mu_e} + \left( \frac{\partial \mu_e}{\partial \mu_{\nu_e}} \right)_{\rho, T} \left( \frac{\partial P}{\partial \mu_e} \right)_{\rho, T, \mu_{\nu_e}} \simeq n Y_{\nu_e} + n Y_e = n Y_L. \quad (\text{B12})$$

Driving from radiative diffusion therefore occurs if

$$\kappa_{\text{eff}} \left[ \frac{\pi^2}{3} \left( \frac{k_B T}{\epsilon_F} \right) \left[ Y_n^{1/3} + Y_p^{1/3} \right] + Y_e \right] \times \frac{1}{2} \gtrsim \kappa_0 \pi^2 Y_L^2 \quad (\text{B13})$$

which is marginally satisfied for  $k_B T \gtrsim 20$  MeV and/or  $\rho \lesssim 10^{14}$  g cm $^{-3}$ .

## APPENDIX C: CHEMICAL AND THERMAL EQUILIBRIUM

### CHEMICAL AND THERMAL SOURCE TERMS

In order to calculate the conditions for chemical and thermal equilibrium, we must linearize the Boltzmann equation for all six ( $n, p, e^-, e^+, \nu_e, \bar{\nu}_e$ ) particle species. Electron (beta) capture is the inelastic radiative process that mediates chemical and thermal balance i.e.,

$$e^- + p \rightleftharpoons n + \nu_e \quad (\text{D1})$$

$$e^+ + n \rightleftharpoons p + \bar{\nu}_e. \quad (\text{D2})$$

In order to close our set of equations and for the sake of simplicity, we make five simplifying assumptions before doing so:

- All species are represented, to lowest order, by a Fermi-Dirac distribution function characterized by an individual temperature and chemical potential. For example, in the case of protons

$$f_p = \frac{1}{e^{(E_p - \mu_p)/k_B T_p} + 1}. \quad (\text{D3})$$

- Thermal equilibrium for the background state,

$$T_p = T_n = T_{e^-} = T_{e^+} = T_{\nu_e} = T_{\bar{\nu}_e} = T. \quad (\text{D4})$$

- Chemical equilibrium for the background state,

$$\frac{\mu_p + \mu_e - \mu_n}{k T_g} - \frac{\mu_{\nu_e}}{k T_{\nu_e}}. \quad (\text{D5})$$

- Due to strong and electromagnetic interactions

$$\delta T_{e^-} = \delta T_{e^+} = \delta T_p = \delta T_n = \delta T_g \quad (\text{D6})$$

and

$$\delta T_{\nu_e} = \delta T_{\bar{\nu}_e}. \quad (\text{D7})$$

- The last assumption is that the medium is sufficiently hot and optically thick such that  $E_e \simeq E_{\nu} \gg (m_n - m_p)c^2$ .

Now, consider the evolution of the partial fraction  $Y_{e^-}$  mediated by the reaction  $e^- + p \rightarrow n + \nu_e$ , governed by the Boltzmann equation

$$n \left( \frac{dY_{e^-}}{dt} \right)_{\text{capture}} = - \frac{G_F^2}{\pi (\hbar c)^4} \frac{(g_V^2 + 3g_A^2)}{(2\pi)^3} \frac{2\pi c}{(\hbar c)^3} \frac{2}{h^3 c^3} \int d^3 p_p \frac{2}{h^3 c^3} \int d^3 p_n \int_0^\infty dE_0 E_0^2 d\mu_0 E_0^2 f_p (1-f_n) f_e (1-f_{\nu_e}) \quad (\text{D8})$$

where  $E_0$  is the electron energy. At the same time, we must consider electron emission via neutrino capture via the reaction  $\nu_e + n \rightarrow e^- + p$ . This gives us

$$n \left( \frac{dY_{e^-}}{dt} \right)_{\text{emission}} = + \frac{G_F^2}{\pi (\hbar c)^4} \frac{(g_V^2 + 3g_A^2)}{(2\pi)^3} \frac{2\pi c}{(\hbar c)^3} \frac{2}{h^3 c^3} \int d^3 p_p \frac{2}{h^3 c^3} \int d^3 p_n \int_0^\infty dE_0 E_0^2 d\mu_0 E_0^2 f_n (1-f_p) f_{\nu_e} (1-f_e). \quad (\text{D9})$$

After a quick algebraic manipulation, we may write the familiar expression

$$\begin{aligned} n \frac{dY_{e^-}}{dt} &= \left( \frac{dY_{e^-}}{dt} \right)_{\text{capture}} - \left( \frac{dY_{e^-}}{dt} \right)_{\text{emission}} \\ &= - \frac{G_F^2}{\pi (\hbar c)^4} \frac{(g_V^2 + 3g_A^2)}{(2\pi)^3} \frac{2\pi c}{(\hbar c)^3} \times \\ &\quad \frac{2}{h^3 c^3} \int d^3 p_p \frac{2}{h^3 c^3} \int d^3 p_n \int_0^\infty dE_0 d\mu_0 E_0^4 f_p (1-f_n) f_e (1-f_{\nu_e}) \times \left( 1 - e^{\frac{E_p + E_e - E_n}{kT_g} - \frac{E_{\nu_e}}{kT_{\nu_e}} + \frac{\mu_n - \mu_p - \mu_e}{kT_g} + \frac{\mu_{\nu_e}}{kT_{\nu_e}}} \right). \end{aligned} \quad (\text{D10})$$

Note that the term in the exponential on the right hand side is equal to zero in equilibrium.

Now we can consider perturbations. By applying energy conservation we have

$$\begin{aligned} n \delta \frac{dY_{e^-}}{dt} &= + \frac{G_F^2}{\pi (\hbar c)^4} \frac{(g_V^2 + 3g_A^2)}{(2\pi)^3} \frac{2\pi c}{(\hbar c)^3} \frac{2}{h^3 c^3} \int d^3 p_p \frac{2}{h^3 c^3} \int d^3 p_n \int_0^\infty dE_0 d\mu_0 E_0^4 f_p (1-f_n) f_e (1-f_{\nu_e}) \\ &\quad \times \left[ \left( \frac{E_0 - \mu_{\nu_e}}{kT^2} \right) \times (\delta T_g - \delta T_{\nu_e}) + \frac{1}{kT} (\delta \mu_p + \delta \mu_e - \delta \mu_{\nu_e} - \delta \mu_n) \right]. \end{aligned} \quad (\text{D11})$$

If we neglect the final state blocking of the baryons, we are left with

$$\delta \frac{dY_{e^-}}{dt} = + \frac{G_F^2}{\pi (\hbar c)^4} \frac{(g_V^2 + 3g_A^2)}{(2\pi)^3} \frac{4\pi c Y_p}{(\hbar c)^3} \int_0^\infty dE_0 E_0^4 f_e (1-f_{\nu_e}) \left[ \left( \frac{E_0 - \mu_{\nu_e}}{kT^2} \right) \times (\delta T_g - \delta T_{\nu_e}) + \frac{1}{kT} (\delta \mu_p + \delta \mu_e - \delta \mu_{\nu_e} - \delta \mu_n) \right]. \quad (\text{D12})$$

This integral can easily be calculated by making use of the relation

$$f(x_1)(1-f(x_2)) = \frac{f(x_1) - f(x_2)}{1 - e^{x_1 - x_2}}. \quad (\text{D13})$$

The expression for electron evolution becomes

$$\begin{aligned} -i\omega \delta Y_{e^-} + \delta \mathbf{v} \cdot \nabla Y_{e^-} &= - \frac{c \tilde{\sigma}_0}{8\pi^2} \left( \frac{kT}{m_e c^2} \right)^2 \left( \frac{kT}{\hbar c} \right)^3 \frac{Y_p}{1 - e^{y/kT}} \times \\ &\quad \left[ \left( \frac{\delta T_g - \delta T_{\nu_e}}{T} \right) [F_5(\eta_e) - F_5(\eta_{\nu_e})] + \left( \frac{\delta \mu_p + \delta \mu_e - \delta \mu_n - \delta \mu_{\nu_e}}{kT} - \frac{\mu_{\nu_e}}{kT} \frac{\delta T_g - \delta T_{\nu_e}}{T} \right) [F_4(\eta_e) - F_4(\eta_{\nu_e})] \right] \end{aligned} \quad (\text{D14})$$

where

$$\begin{aligned} \tilde{\sigma}_0 &\equiv \sigma_0 (g_V^2 + 3g_A^2) \\ G_F^2 &= \frac{\pi \sigma_0}{4} \frac{(\hbar c)^4}{(m_e c^2)^2} \\ y &\equiv \mu_{\nu_e} - \mu_e \\ F_n(\eta) &= \int_0^\infty dx \frac{x^n}{e^{x-\eta} + 1}. \end{aligned} \quad (\text{D15})$$

If we wish to follow the evolution of the total electron fraction  $Y_e = Y_{e^-} - Y_{e^+}$  where the evolution of the  $e^+$ s are mediated by the reactions  $e^+ + n \rightleftharpoons p + \bar{\nu}_e$ , then the relevant expression becomes

$$\begin{aligned} -i\omega \delta Y_e + \delta \mathbf{v} \cdot \nabla Y_e &= - \frac{c \tilde{\sigma}_0}{8\pi^2} \left( \frac{kT}{m_e c^2} \right)^2 \left( \frac{kT}{\hbar c} \right)^3 \frac{Y_p}{1 - e^{y/kT}} \times \\ &\quad \left[ \left( \frac{\delta T_g - \delta T_{\nu_e}}{T} \right) [D_5(\eta_e) - D_5(\eta_{\nu_e})] + \left( \frac{\delta \mu_p + \delta \mu_e - \delta \mu_n - \delta \mu_{\nu_e}}{kT} - \frac{\mu_{\nu_e}}{kT} \frac{\delta T_g - \delta T_{\nu_e}}{T} \right) [D_4(\eta_e) - D_4(\eta_{\nu_e})] \right] \end{aligned} \quad (\text{D16})$$

and the expression for conservation of electron neutrino fraction, which is defined as  $Y_{\nu_e} \equiv Y_{\nu_e} - Y_{\bar{\nu}_e}$ , reads

$$\begin{aligned} -i\omega \delta Y_{\nu_e} + \delta \mathbf{v} \cdot \nabla Y_{\nu_e} &= + \frac{c \tilde{\sigma}_0}{8\pi^2} \left( \frac{kT}{m_e c^2} \right)^2 \left( \frac{kT}{\hbar c} \right)^3 \frac{Y_p}{1 - e^{y/kT}} \times \left\{ \left( \frac{\delta T_g - \delta T_{\nu_e}}{T} \right) [D_5(\eta_e) - D_5(\eta_{\nu_e})] \right. \\ &\quad \left. + \left( \frac{\delta \mu_p + \delta \mu_e - \delta \mu_n - \delta \mu_{\nu_e}}{kT} - \frac{\mu_{\nu_e}}{kT} \frac{\delta T_g - \delta T_{\nu_e}}{T} \right) [D_4(\eta_e) - D_4(\eta_{\nu_e})] \right\} - \frac{i}{n_B} \mathbf{k} \cdot \delta \mathbf{F}_L \end{aligned} \quad (\text{D17})$$

where we have defined

$$D_n \equiv F(\eta) - F(-\eta). \quad (\text{D18})$$

The energy source term for the electrons is calculated in a very similar manner. To be clear, the first law of thermodynamics for the electrons may be written as

$$\begin{aligned} \frac{dU_{e^-}}{dt} + (U_{e^-} + P_{e^-}) \nabla \cdot \mathbf{v} = S_{e^-} = & -\frac{G_F^2}{\pi (\hbar c)^4} \frac{(g_V^2 + 3g_A^2)}{(2\pi)^3} \frac{2\pi c}{(\hbar c)^3} \times \\ & \frac{2}{h^3 c^3} \int d^3 p_p \frac{2}{h^3 c^3} \int d^3 p_n \int_0^\infty dE_0 d\mu_0 E_0^5 f_p (1 - f_n) f_e (1 - f_{\nu_e}) \times \left( 1 - e^{\frac{E_p + E_e - E_n}{kT_g} - \frac{E_{\nu_e}}{kT_{\nu_e}} + \frac{\mu_n - \mu_p - \mu_e}{kT_g} + \frac{\mu_{\nu_e}}{kT_{\nu_e}}} \right). \end{aligned} \quad (\text{D19})$$

Upon perturbations, conservation of energy per unit volume for the the electrons is expressed by

$$\begin{aligned} -i\omega \delta U_{e^-} + \delta \mathbf{v} \cdot \nabla U_{e^-} + (U_{e^-} + P_{e^-}) \nabla \cdot \delta \mathbf{v} = & -\frac{c \tilde{\sigma}_0}{8\pi^2} \left( \frac{kT}{m_e c^2} \right)^2 \frac{(kT)^4}{(\hbar c)^3} \frac{n_p}{1 - e^{y/kT}} \times \left\{ \left( \frac{\delta T_g - \delta T_{\nu_e}}{T} \right) [F_6(\eta_e) - F_6(\eta_{\nu_e})] \right. \\ & \left. + \left( \frac{\delta \mu_p + \delta \mu_e - \delta \mu_n - \delta \mu_{\nu_e}}{kT} - \frac{\mu_{\nu_e}}{kT} \frac{\delta T_g - \delta T_{\nu_e}}{T} \right) [F_5(\eta_e) - F_5(\eta_{\nu_e})] \right\}. \end{aligned} \quad (\text{D20})$$

Note that the source term which drives electrons into thermal equilibrium is *not exactly equal* to the source term which drives the electrons into chemical equilibrium even though they are comparable in both appearance and magnitude. This is of importance when considering a spectrum of perturbations in the upper layer of a proto-neutron star. For a given dynamical timescale, the depth beneath the neutrinosphere at which the the fluctuations are in chemical equilibrium may differ, in principle, from the layer in which thermal equilibrium is achieved. In terms of neutrino bubble driving, whether or not the perturbations are either in chemical or thermal equilibrium or both, will determine whether or not driving due to changes in neutrino chemical potential (or the lepton flux) or driving due to changes in neutrino temperature (or the radiative flux) dominate the mechanics of the instability.

The first law for the combined electron, positron, neutron, and proton gas is given by

$$\begin{aligned} -i\omega \delta U_g + \delta \mathbf{v} \cdot \nabla U_g + (U_g + P_g) \nabla \cdot \delta \mathbf{v} = & -\frac{c \tilde{\sigma}_0}{8\pi^2} \left( \frac{kT}{m_e c^2} \right)^2 \frac{(kT)^4}{(\hbar c)^3} \frac{n_p}{1 - e^{y/kT}} \times \left\{ \left( \frac{\delta T_g - \delta T_{\nu_e}}{T} \right) [C_6(\eta_e) - C_6(\eta_{\nu_e})] \right. \\ & \left. + \left( \frac{\delta \mu_p + \delta \mu_e - \delta \mu_n - \delta \mu_{\nu_e}}{kT} - \frac{\mu_{\nu_e}}{kT} \frac{\delta T_g - \delta T_{\nu_e}}{T} \right) [C_5(\eta_e) - C_5(\eta_{\nu_e})] \right\} \end{aligned} \quad (\text{D21})$$

where

$$\begin{aligned} U_g &\equiv U_n + U_p + U_e \quad \text{and} \quad U_e \equiv U_{e^-} + U_{e^+} \\ P_g &\equiv P_n + P_p + P_e \quad \text{and} \quad P_e \equiv P_{e^-} + P_{e^+} \\ C_n(\eta) &\equiv F_n(\eta) + F_n(-\eta). \end{aligned} \quad (\text{D22})$$

For the electron type neutrino's, the first law of thermodynamics reads

$$\begin{aligned} -i\omega \delta U_{\nu_e} + \delta \mathbf{v} \cdot \nabla U_{\nu_e} + (U_{\nu_e} + P_{\nu_e}) \nabla \cdot \delta \mathbf{v} = & +\frac{c \tilde{\sigma}_0}{8\pi^2} \left( \frac{kT}{m_e c^2} \right)^2 \frac{(kT)^4}{(\hbar c)^3} \frac{n_p}{1 - e^{y/kT}} \times \left\{ \left( \frac{\delta T_g - \delta T_{\nu_e}}{T} \right) [C_6(\eta_e) - C_6(\eta_{\nu_e})] \right. \\ & \left. + \left( \frac{\delta \mu_p + \delta \mu_e - \delta \mu_n - \delta \mu_{\nu_e}}{kT} - \frac{\mu_{\nu_e}}{kT} \frac{\delta T_g - \delta T_{\nu_e}}{T} \right) [C_5(\eta_e) - C_5(\eta_{\nu_e})] \right\} - i \mathbf{k} \cdot \delta \mathbf{F} \end{aligned} \quad (\text{D23})$$

where now  $U_{\nu_e} \equiv U_{\nu_e} + U_{\bar{\nu}_e}$  and  $P_{\nu_e} \equiv P_{\nu_e} + P_{\bar{\nu}_e}$ . Notice that we have not included the non-electronic type neutrinos in this discussion. The only mechanism which thermodynamically couples the  $\mu$ - and  $\tau$ -type neutrinos to the other fluid and radiation components is inelastic scattering with electrons, in other words, the inverse Compton effect. This coupling is heavily blocked by the final state occupancy of the electrons which reduces the scattering cross-section by a factor of  $(1 - f_e)$ .

#### CHARACTERISTIC TIMESCALES FOR CHEMICAL AND THERMAL EQUILIBRIUM

Timescales for both chemical and thermal equilibrium dictate whether or not the source terms represented in eqs. (D16) and (D21) vanish. That is, electron capture and emission dictate *both* chemical and thermal equilibrium simultaneously.

In order to calculate the magnitude of the lepton source term in eq. (D16), it is convenient to write the left hand side as

$$-i\omega \delta Y_e + \delta \mathbf{v} \cdot \nabla Y_e = -i\omega \left[ \left( \frac{\partial Y_e}{\partial T_g} \right)_{\eta_e, \rho} \delta T_g + \left( \frac{\partial Y_e}{\partial \eta_e} \right)_{T_g, \rho} \delta \eta_e + \left( \frac{\partial Y_e}{\partial \rho} \right)_{T_g, \eta_e} \delta \rho \right] + \delta \mathbf{v} \cdot \nabla Y_e. \quad (\text{E1})$$

Thus, the source of electrons will vanish if

$$\omega_{Y, \text{th}} \equiv \frac{c \sigma_a n_0 Y_p}{T \left( \partial Y_e / \partial T_g \right)_{\eta_e, \rho}} \times \frac{[D_5(\eta_e) - D_5(\eta_{\nu_e})]}{1 - e^{y/kT}} \gg \omega \quad (\text{E2})$$

and

$$\omega_{Y,\text{chem}} \equiv \frac{c\sigma_a n_0 Y_p}{(\partial Y_e / \partial \eta_e)_{T_g, \rho}} \times \frac{[D_4(\eta_e) - D_4(\eta_{\nu_e})]}{1 - e^{y/kT}} \gg \omega \quad (\text{E3})$$

where we have defined

$$\begin{aligned} \sigma_a &\equiv \frac{\tilde{\sigma}_0}{8\pi^2} \left( \frac{kT}{m_e c^2} \right)^2 \\ n_0 &\equiv \left( \frac{k_B T}{\hbar c} \right)^3 \end{aligned} \quad (\text{E4})$$

where  $\sigma_a$  is the characteristic absorption opacity and  $n_0$  is a characteristic relativistic particle number density. Note that the expression for  $\omega_{Y,\text{th}}$  was obtained by rewriting the condition for chemical equilibrium as

$$\frac{\delta\mu_p + \delta\mu_e - \delta\mu_n + \delta\mu_{\nu_e}}{kT} - \frac{\mu_{\nu_e}}{kT} \frac{\delta T_g - \delta T_{\nu_e}}{T} = \delta\eta_p + \delta\eta_e - \delta\eta_n - \delta\eta_{\nu_e}. \quad (\text{E5})$$

Likewise, in order to calculate the net effect of the energy source term in eq. (D21), it is useful to write the left hand side as

$$-i\delta U_g + \delta \mathbf{v} \cdot \nabla U_g + i(U_g + P_g) \mathbf{k} \cdot \delta \mathbf{v} = -i \left[ \left( \frac{\partial U_g}{\partial T_g} \right)_{\eta_e, \rho} \delta T_g + \left( \frac{\partial U_g}{\partial \eta_e} \right)_{T_g, \rho} \delta \eta_e + \left( \frac{\partial U_g}{\partial \rho} \right)_{T_g, \eta_e} \delta \rho \right] + \delta \mathbf{v} \cdot \nabla U_g + i(U_g + P_g) \mathbf{k} \cdot \delta \mathbf{v}. \quad (\text{E6})$$

The heat source for the  $npe\gamma$  gas will vanish if

$$\omega_{U,\text{th}} \equiv \frac{c\sigma_a n Y_p U_0}{T(\partial U_g / \partial T_g)_{\eta_e, \rho}} \times \frac{[C_6(\eta_e) - C_6(\eta_{\nu_e})]}{1 - e^{y/kT}} \gg \omega \quad (\text{E7})$$

and

$$\omega_{U,\text{chem}} \equiv \frac{c\sigma_a n Y_p U_0}{(\partial U_g / \partial \eta_e)_{T_g, \rho}} \times \frac{[C_5(\eta_e) - C_5(\eta_{\nu_e})]}{1 - e^{y/kT}} \gg \omega \quad (\text{E8})$$

where

$$U_0 \equiv \frac{k_B^4 T^4}{\hbar^3 c^3} \quad (\text{E9})$$

serves as a characteristic energy density for relativistic particles. The equilibration rate  $\omega_{Y,\text{chem}}$ , given by eq. (E3), is identical to that derived by Burrows & Lattimer (1986, their eq. 16) except for the presence of a factor  $(\partial Y_e / \partial \eta_e)_{T_g, \rho}$  in the denominator and the absence of a term that drives the system into statistical equilibrium in the numerator. Both discrepancies can be readily accounted for by realizing that our analysis is concerned with perturbations about an equilibrium already in statistical and thermal balance, while those authors calculate whether or not their equilibrium is in statistical and thermal balance with respect to the contraction timescale.

In what follows, we approximate whether or not acoustic-type fluctuations near the neutrinosphere are in chemical and thermal equilibrium. We conclude that chemical and thermal balance between the radiation and gas is marginally satisfied at the neutrinosphere.

#### REQUIREMENTS FOR CHEMICAL AND THERMAL EQUILIBRIUM NEAR THE NEUTRINOSPHERE

Interestingly, the chemical and energy source terms which lead to the characteristic frequencies  $\omega_{Y,\text{th}}$  and  $\omega_{U,\text{th}}$  vanish. This results from the mathematical fact that  $F_n(\eta)$  is an even function if  $n$  is odd and an odd function if  $n$  is even. From a more physical point of view, chemical and thermal balance *simultaneously occur* as long as eq. (E5) is equal to zero.

Throughout the star, from the core to the neutrinosphere, the electrons can be considered fully degenerate such that  $\eta_e \gg 1$ . The thermal contribution to the electrons is more profound near the neutrinosphere, but there,  $\eta_e$  is still  $\gtrsim$  a few. Thus, the Fermi-Dirac integrals for the electrons  $F_n(\eta_e)$  can be approximated as (Pathria 1996)

$$F_n(\eta_e) \simeq \frac{\Gamma(n+1)}{\Gamma(n+2)} \eta_e^{n+1} = \frac{\eta_e^{n+1}}{n+1}, \quad (\text{F1})$$

especially if  $n$  is large. Note that  $\Gamma(n)$  is the Euler Gamma function. Also, near the neutrinosphere, the chemical potential of the electron-type neutrinos  $\mu_{\nu_e} \sim$  a few times smaller than  $\mu_e$ . As a result, we may write

$$\begin{aligned} \omega_{Y,\text{chem}} &\simeq \frac{2}{5} \times \frac{c\sigma_a n_0 Y_p}{(\partial Y_e / \partial \eta_e)_{T_g, \rho}} \eta_e^5 \\ \text{and } \omega_{U,\text{chem}} &\simeq \frac{1}{3} \times \frac{c\sigma_a n Y_p U_0}{T(\partial U_g / \partial T_g)_{\eta_e, \rho}} \eta_e^6. \end{aligned} \quad (\text{F2})$$

Putting in numerical values typical for conditions at and around the neutrinosphere allows us to write the characteristic frequencies for chemical and thermal equilibrium in terms of  $Y_e$ ,  $T$ , and  $\mu_e$ ,

$$\begin{aligned} \omega_{Y,\text{chem}} &\simeq 3 \times 10^4 \frac{\mu_{20}^6}{T_4} \text{ s}^{-1} \\ \omega_{U,\text{chem}} &\simeq 2 \times 10^4 Y_{1/3} \frac{\mu_{20}^6}{T_4} \text{ s}^{-1} \end{aligned} \quad (\text{F3})$$

where  $Y_{1/3}$ ,  $T_4$ , and  $\mu_{20}$  are the electron fraction in units of  $1/3$ , temperature in units  $4 \text{ MeV}$ , and electron chemical potential normalized to  $20 \text{ MeV}$ , respectively. In the above formulae, we made the approximation that the gas is primarily supported by the thermal pressure of the baryons. At the neutrinosphere, the sound crossing time  $\sim 0.1 \text{ ms}$ , implying that chemical and thermal equilibrium is marginally satisfied for acoustic-type oscillations.<sup>12</sup>

<sup>12</sup> If the atmosphere is dominated by magnetic pressure, the acoustic time for the fast magnetosonic wave is shorter than that of ordinary sound waves. Even if this were the case, the slow magnetosonic wave is the excitation species of interest since it always has larger growth rates than the fast wave (BS03).